Tc1 and Th1 T-lymphocyte rich tumor microenvironment is a hallmark of MSI colorectal cancer

Dissertation

zur Erlangung des akademischen Grades eines
Doktors der Medizin (Dr. med.)

an der

Medizinischen Fakultät der Universität Hamburg

vorgelegt von

Zhihao Huang

Aus

China

2024

Betreuer:in / Gutachter:in der Dissertation: Prof. Dr. Guido Sauter

Gutachter:in der Dissertation: Prof. Dr. Nicola Gagliani

Vorsitz der Prüfungskommission: Prof. Dr. Nicola Gagliani

Mitglied der Prüfungskommission: Prof. Dr. Ronald Simon

Mitglied der Prüfungskommission: Prof. Dr. Thilo Welsch

Datum der mündlichen Prüfung: 16.09.2025

Table of contents

1. Hypothesis and Research Question

Colorectal cancer is the tumor entity with the highest degree of microsatellite instability (MSI) ranging from 12% to 20% of cases (1,2). Microsatellite instable colorectal cancers are well known for its strong link to favorable patient outcome (3), increased response to immune checkpoint inhibitors(4), high mutational burden(5), poor differentiation(6), and an inflamed immune phenotype(7). Moreover, recent evidence suggests that the interdependencies between subpopulations of cytotoxic T-cells, such as type 1 cytotoxic T-cells (Tc1), and subpopulations of helper T-cells, such as type 1 T-helper cells (Th1), type 2 T-helper cells (Th2), type 17 T-helper cells (Th17), and regulatory T-cells (Tregs) highly impact the efficacy of anti-cancer immunity depending on the microsatellite status(7,8). However, the alterations of the T-cell composition and underlying changes in the immune tumor microenvironment that lead to such favorable patient outcomes are still unknown.

Microsatellite instability in colorectal cancer is associated with increased infiltration of $CD8^+$ cytotoxic T cells, particularly Tc1, leading to enhanced tumor cell destruction (8,9). Functional analysis has shown that Tc1 represent the main component of the terminal-end-route of anticancer immunity by producing high levels of cytolytic cytokines such as perforin, INF-γ and granzyme B, thus initiating direct tumor cell killing (8,10), while other cytotoxic T-cell subsets such as type 2 (Tc2)(8,11), or regulatory cytotoxic T-cells (Tcreg)(12) contribute less effectively to tumor cell destruction. Furthermore, it has been shown that Th1 can enhance Tc1 effector function by targeted delivery of cytokines via acquired pMHC I complexes (13). In addition, Th1 is also well known for robust secretion of IFN-γ and chemokines, facilitating the priming and proliferation of $CD8^+$ T-cell subpopulations (14,15). The role of Th2 and Th17 in the tumor microenvironment of colorectal cancer is more contradictory. Th2 has been found to promote tumor growth in colorectal cancer (16) but also shows anti-tumor activity due to its cytokine secretion profile (17). Although a high fraction of Th17 was linked to tumor progression due to the promotion of intestinal tumorigenesis (18,19) and angiogenesis by IL-17 expression (20), anticancer functions such as promoting localization of highly cytotoxic $CD8^+$ T-cells to tumor tissues have been also described (21). In addition, regulatory T-cells (Tregs) appear to mitigate inflammatory damage and may suppress anti-cancer immune responses during different stages of carcinogenesis in colorectal cancer (22).

Therefore, the hypothesis of study is that the alterations of the T-cell composition and underlying changes in the immune tumor microenvironment contribute to favorable patient outcomes in MSI compared to MSS colorectal cancers. The research question is how do the composition, functional marker expression, and spatial interactions of T-cell subpopulations differ between microsatellite instability (MSI) and microsatellite stable (MSS) colorectal cancers.

2. Introduction

2.1 Colorectal cancer

Colorectal cancer (CRC), which affects the colon and/or rectum, is a major health concern worldwide, ranking as the third most diagnosed and the second most fatal cancer globally (https://www.who.int/news-room/fact-sheets/detail/cancer). In 2020, GLOBOCAN data estimated 19.3 million new cancer cases and 10 million cancer deaths globally, with CRC contributing approximately 1.93 million cases (10%) and 0.94 million deaths(23). Among CRC cases, colon cancer is predominant, accounting for 59.5% of new cases and 61.9% of deaths, while rectal cancer constitutes 37.9% of incidences and 36.3% of mortality across genders and age groups(23). Although CRC-related deaths are high in high-income countries, the incidence and mortality rates are rising in developing regions as well. CRC is influenced by environmental and genetic factors, with risks increasing with age, particularly in patients with longstanding ulcerative colitis or Crohn's disease(24). Additional risk factors include dietary and lifestyle choices, family history, and chronic inflammation(25).

CRC classification encompasses histological subtype, tumor location, mutation origin, and molecular pathways. Histologically, CRC is categorized into adenocarcinoma, neuroendocrine tumor, neuroendocrine carcinoma, and mixed neuroendocrine-nonneuroendocrine neoplasm, with adenocarcinoma comprising over 90% of cases worldwide (26,27). Subtypes of colorectal adenocarcinoma include mucinous, medullary, and signet ring cell types(26,27). Based on location, colon cancer is divided into proximal (midgut origin) and distal (hindgut origin) types, with distal colon cancer generally showing a more favorable prognosis than proximal colon cancer(28). CRC can also be classified by the mutation origin, with three main categories: sporadic CRC (70%), familial CRC (25%), and inherited CRC (5%) (28,29). Molecular pathway classifications include chromosomal instability (CIN), microsatellite instability (MSI), and CpG island methylator phenotype (CIMP) pathways(30). In 2015, the CRC Subtyping Consortium developed a unified molecular classification system known as the Consensus Molecular Subtypes (CMS), based on 4,151 CRC samples, to reflect CRC's heterogeneity. This system includes four subtypes: CMS1 (MSI Immune, 14%) with high immune activation and best survival in local disease, CMS2 (Canonical, 37%) with chromosomal instability and good prognosis, CMS3 (Metabolic, 13%) showing metabolic dysregulation, and CMS4 (Mesenchymal, 23%) with stromal invasion and the poorest prognosis(30,31).

Screening is the most effective strategy to prevent CRC and reduce mortality among average-risk individuals(25). Many countries in Europe, Canada, and parts of North and South America, Asia, and Oceania have implemented population-based screening programs(32). Eligibility to participate in CRC screening is determined by age and area of residence. The results of microsimulation modeling have shown a decline in CRC cases and deaths in the United States, largely attributed to such screening initiatives(25). Screening identifies early-stage disease, enabling timely intervention and reducing

CRC's threat to individuals and communities. CRC's gradual adenoma-to-carcinoma progression, typically taking at least ten years, provides a window for early detection and treatment(33). Removal of precancerous polyps can prevent CRC(34), and early detection significantly improves survival outcome(35). Additional preventive measures include targeting high-risk groups, such as those with inflammatory bowel disease, hereditary CRC syndromes, family histories indicating genetic predisposition, and phenotypically high-risk individuals. Recent advances in metabolomics help identify the biological pathways impacted by genetic variation(36). The primary screening methods for CRC are fecal occult blood tests (FOBTs) and lower endoscopy(37).

2.2 Microsatellite instability in colorectal cancers

Microsatellite instability (MSI) is a hypermutable phenotype resulting from impaired DNA mismatch repair (MMR) activity(38). The MMR system plays a crucial role in correcting replication errors in DNA, particularly in repetitive sequences called microsatellites(39). Four main genes regulate the MMR mechanism: MLH1, MSH2, MSH6, and PMS2. Biallelic inactivation of these genes, caused by mutations or epigenetic changes, leads to deficient MMR (dMMR). This deficiency increases replication errors, causing mutations that alter the sequence length of microsatellites, a condition referred to as microsatellite instable (MSI). MSI tumors accumulate numerous mutations due to this defective repair syste(38). If tumor tissues do not exhibit changes or instability at microsatellite loci, then they are microsatellite stable (MSS) tumors.

Colorectal cancer (CRC) exhibits the highest rates of MSI among cancer types, occurring in 12% to 20% of cases (1,2). Approximately 3% of MSI cases are linked to Lynch syndrome (hereditary), while 12% arise sporadically, often due to MLH1 promoter hypermethylatio(38). Several detection methods are established to identify MSI colorectal cancers, mainly including polymerase chain reaction (PCR)-based methods, immunohistochemistry (IHC), and next-generation sequencing (NGS). A commonly used method combines fluorescent multiplex PCR with capillary electrophoresis (CE) to detect MSI across five quasi-monomorphic sites (BAT-26, NR-21, BAT-25, MONO-27, and NR-24) in a single test, providing high sensitivity and reliable results(40). IHC, another detection approach, assesses MMR protein expression (hMLH1, hPMS2, hMSH2, and hMSH6); absence of any MMR protein indicates dMMR, while presence of all four suggests proficient mismatch repair (pMMR)(41). In general, dMMR is equivalent to MSI-H(42). Though IHC is straightforward and often preferred, it may yield discordant results compared to PCR in some cases. For instance, MSH6 mutation may result in dMMR without meeting MSI-high (MSI-H) criteria, while MSI-H status can sometimes exist without detectable MMR protein loss(43,44). To address these discrepancies, studies recommend combining molecular analysis with IHC and MSI testing. However, this dual approach is costly and requires larger sample quantities(45). NGS has emerged as a potential solution, enabling MSI detection alongside MMR gene analysis and tumor mutational burden (TMB) assessment using smaller samples(46). In 2017, MSK's IMPACT and FMI's F1CDx (approved by the FDA in 2018) became notable NGS products

for MSI testing, offering over 92% concordance with traditional methods(47,48).

MSI colorectal cancers (MSI-CRCs) are characterized by distinct features. They are more frequently located in the right (proximal) colon; in one study, 66.7% of tumors in the proximal colon exhibited MSI-H, compared to only 25.7% in distal tumors(49). Although the right-sided location raises suspicion of MSI, molecular confirmation is essential(50). MSI-CRCs are also associated with better patient outcomes. A pooled analysis of 7,642 CRC cases revealed a hazard ratio of 0.65 for MSI-H tumors, with later studies confirming reduced risk of death and relapse for MSI-H stage II CRC(51,52). MSI-CRCs show a heightened response to immune checkpoint inhibitors, particularly in cases of high tumor mutational burden(4,53). Multiple studies support the sensitivity of MSI-CRCs to treatments such as anti-PD-1 and PD-L1 antibodies(54,55). Histologically, MSI-CRCs are often poorly differentiated, displaying mucinous or signet-ring cell patterns(38).

MSI-CRCs have an inflamed immune profile, with diverse T-cell subpopulations like Type 1 cytotoxic T-cells (Tc1) and helper T-cells (Type 1, Type 2, Type 17, and regulatory) affecting immune response based on MSI status(8,56). For instance, a study analyzing the RNA data from TCGA cohort or immunohistochemistry data demonstrates that MSI colorectal cancers exhibit higher densities of type 1 helper T-cells (Th1), effector-memory T-cells, in situ proliferating T-cells, and inhibitory PD1-PDL1 cells, indicating robust immune activity, with mutation-specific cytotoxic T-cell infiltration reflected in high Immunoscore(56).

2.3 Tumor microenvironment in colorectal cancers

Macrophages in colorectal cancer (CRC) exhibit considerable diversity, with subpopulations that serve distinct roles within the tumor microenvironment(57). These cells can polarize into pro-inflammatory (M1) or anti-inflammatory (M2) phenotypes, with M2-like tumor-associated macrophages (TAMs) predominating in the tumor microenvironment(58). Higher ratios of $CD163^+/CD68^+$ macrophages, indicating M2 polarization, are found at the invasive front compared to the tumor center(59). Some studies link higher macrophage infiltration with advanced tumor stages and poor prognosis(60), while others associate TAMs with improved survival and lower risk of liver metastasis, especially in colon cancer(61,62). The impact of TAMs varies by phenotype, tumor location, and interactions within the tumor microenvironment, with M1 macrophages linked to better outcomes and M2 macrophages often associated with worse prognosis(62-64). M2-like TAMs are thought to enhance CRC cell migration, invasion, and metastasis through mechanisms like epithelial-mesenchymal transition (EMT) and the secretion of growth factors and proteases, promoting angiogenesis and immunosuppression(65).

Dendritic cells (DCs) in CRC also play a role in immune modulation, with infiltration levels and distribution linked to tumor stage and metastasis(66). Reduced levels of mature DCs ($CD83^+$) in the tumor stroma and invasive margins correlate with locally advanced and metastatic disease(67).

Increased densities of tumor-infiltrating plasmacytoid DCs (pDCs), however, are associated with longer survival in colon cancer(67). CRC-induced DC dysfunction, often mediated by factors like TGF-β and VEGF, is a critical mechanism of immune evasion, as DCs support anti-tumor immunity. Targeting DC dysfunction may improve treatment outcomes, making them potential candidates for cancer vaccines(68-70)

Myeloid-derived suppressor cells (MDSCs) are expanded in both peripheral blood and tumor tissues of CRC patients, contributing to immune suppression and facilitating cancer progressio(71). Elevated MDSC levels are associated with advanced tumor-node-metastasis (TNM) stages and CRC growth. These cells suppress T-cell proliferation, enhance CRC cell growth, and promote metastasis by creating pre-metastatic niches. MDSCs operate through pathways like JAK-STAT, PI3K, and IL-6, with KRAS mutations driving their migration to the tumor microenvironment through CXCL3-CXCR2 signaling(72). Targeting MDSCs through recruitment inhibition and functional alteration shows potential when combined with chemotherapy, radiotherapy, or immunotherapy(71).

The role of mast cells (MCs) in CRC prognosis is complex, with some studies associating them with better outcomes and others linking them to reduced survival(73,74). MCs can inhibit CRC progression by inducing endoplasmic reticulum stress through Cystatin C secretion, yet they also promote tumor growth via angiogenic factors (VEGF-A, CXCL8, MMP-9) and lymphangiogenic factors (VEGF-C, VEGF-D)(73). MCs contribute to a pro-inflammatory environment, interact with MDSCs, and influence cell motility through RhoA signaling in cancer cells, making them targets for CRC immunotherapy exploration(73).

Cancer-associated fibroblasts (CAFs) are highly prevalent in the CRC tumor microenvironment and play a significant role in CRC progression(75). Originating from pericryptal fibroblasts, CAFs express markers like α-SMA, fibronectin, and P4HA1. They promote CRC cell migration, invasion, and EMT by inducing Leucine Rich Alpha-2-Glycoprotein 1 (LRG1) expression and activating STAT3 signaling through IL-6 secretion(76). CAFs also contribute to liver metastasis and drug resistance in CRC, making them critical targets for anti-tumor therapy. Targeting CAF-induced LRG1/TGFβR1 signaling and stromal interactions, such as IL-1R1, holds promise for reducing metastasis and enhancing treatment effectiveness(77,78).

2.4 T-cell components of the tumor immune microenvironment

2.4.1 Type 1 helper T-cells (Th1)

Th1 cells arise from naïve $CD4^+$ T-cells under the influence of the cytokine interleukin (IL)-12, which activates the STAT1 and STAT4 signaling pathways. These pathways promote the transcription of T-box transcription factor (T-bet), a key regulator of Th1 cell differentiation(79). Th1 cells are distinguished by their production of cytokines, including IFN-γ, TNF-α, monocyte chemotactic protein-1, and macrophage inflammatory protein-1α. Primarily, they mediate immune responses

against intracellular pathogens by enhancing CD8 T-cell activity or activating macrophages to engulf these pathogens(14). Although initially recognized for their role in combating intracellular infections, preclinical tumor models indicate that Th1 cells are crucial for antitumor immunity, exhibiting polyfunctional activity in this context(80). Their presence correlates with favorable clinical outcomes across various cancers, including melanoma, gastric cancer, head and neck squamous cell carcinoma, and non-small cell lung cancer(81-83).

2.4.2 Type 2 helper T-cells (Th2)

Th2 cells are characterized by the transcription factor GATA-3 and secrete key cytokines such as interleukins (IL)-4, -5, and -13. These cells play a role in humoral immunity and are involved in allergic inflammatory responses. IL-4 and IL-13 drive Type II inflammation, which not only weakens Th1 antitumor signaling but also attracts and induces immunosuppressive macrophages(84,85). Additionally, Th2 cells can support tumor metastasis and immune evasion. However, they also recruit cytotoxic eosinophils and arginase-producing macrophages by secreting IL-15(86,87). The presence of Th2 cells is generally associated with poorer clinical outcomes across various cancers, including hepatocellular carcinoma(88), ovarian cancer(89), oropharyngeal cancer(90), and pancreatic adenocarcinoma(91), though some aspects remain debated.

2.4.3 Type 17 helper T-cells (Th17)

The Th17 cell subset relies on the transcription factors STAT3 and RORγt and is primarily characterized by the production of cytokines IL-17A and IL-17F(92). IL-17 plays a dual role in cancer, exhibiting both antitumor and protumor activities. On one hand, IL-17 supports antitumor immunity by recruiting macrophages, neutrophils, NK cells, and $CD8^+$ T-cells, while preventing the accumulation of myeloid-derived suppressor cells(93,94). On the other hand, IL-17 promotes tumor angiogenesis and metastasis, contributing to tumor progression(95,96). Th17 cells display significant plasticity, with some cells differentiating further into IFN-γ–secreting effector cells that produce chemokines like CXCL9 and CXCL10, enhancing effector cell recruitment to the tumor microenvironment(85,97). However, Th17 cells can also contribute to tumor growth through the secretion of regulatory cytokines IL-10 and TGF-β. The prognostic impact of Th17 cells is complex and varies across cancers. Th17 cells have been linked to improved prognosis in cancers such as breast(94), cervical(98), hepatocellular(99), and gastric cancers(100). Conversely, they are associated with worse outcomes in breast(101), cervical(102), esophageal(103), lung(104), and prostate cancers(105).

2.4.4 Follicular helper T-cells (Tfh)

Follicular helper T (Tfh) cells are defined by their capacity to migrate to follicles in secondary lymphoid organs, where they interact with B cells to support their differentiation into antibody-secreting cells. Key features of Tfh cells include surface expression of CXC chemokine receptor 5 (CXCR5 or CD185), inducible T-cell costimulator, and programmed cell death protein 1 (PD-1), along with the secretion of IL-21. The transcription factor Bcl-6 is essential for Tfh cell function, guiding the

genetic programming specific to these cells(14). Tfh cells produce IL-21 and CXCL13, which not only aid in B-cell maturation and antibody production but also contribute to the formation and maintenance of tertiary lymphoid structures (TLSs)(106). The presence of Tfh cells is associated with favorable prognosis across various cancers, including adenocarcinoma(107), breast(108), and bladder(109).

2.4.5 Regulatory helper T-cells (Treg)

Regulatory T-cells (Tregs) are defined by their expression of the Foxp3 transcription factor. Evidence suggests that tumor-derived factors can promote the recruitment and expansion of $Foxp3^+$ Tregs within the tumor environment. While $Foxp3^+$ Tregs typically make up 5% to 10% of CD4 T-cells in peripheral lymphoid tissues, their proportion can rise to 20% to 30% in tumor settings, varying by tumor type(110). Tregs express CD25, which allows them to consume IL-2, a cytokine critical for the growth and survival of effector T-cells. By limiting IL-2 availability, Tregs can suppress other immune cells, including $CD8^+$ T-cells, NK cells, Th1, and Th17 cells, thereby aiding tumor immune evasion(111,112). Additionally, Tregs produce IL-10 and TGF-β, which further inhibit antitumor functions of Th1 and Th17 cells and facilitate tumor progression(113). The presence of Tregs is associated with poorer clinical outcomes across various cancers, including breast(114), lun(115), and ovarian cancers(116).

2.4.6 Type 1 cytotoxic T-cells (Tc1)

Tc1 cells, a subset of cytotoxic $CD8^+$ T-cells, produce perforin, granzyme B, IFN-γ, and TNF-α, which equip them to target and destroy tumor or infected cells. Tc1 cell activation is driven by IL-12, which is secreted by antigen-presenting cells exposed to pathogen-related stimuli. Key transcription factors, including STAT4, T-bet, and EOMES, are essential for Tc1 cell polarization(8). Traditionally, activated Tc1 cells eliminate their targets through perforin-granzyme and Fas-FasL signaling pathways.

Tc1 cells are the most common tumor-infiltrating lymphocytes in cancers such as lung cancer(117), breast cancer(118), and chronic lymphocytic leukemia(119), and are associated with improved prognoses(120,121). Tumors with high Tc1 cell infiltration and subsequent IFN-γ production are known as “hot” tumors, which respond more favorably to immunotherapies compared to “cold” tumors lacking Tc1 infiltration(122,123). In melanoma patients, CD29 expression has been linked to increased Tc1 cell cytotoxicity, making CD29 a potential marker for their cytotoxic strength(124).

2.4.7 Type 2 cytotoxic T-cells (Tc2)

A subset of $CD8^+$ T-cells known as Tc2 cells, which produce Th2-associated cytokines, is commonly found in airway and intraepithelial tissues(125). When naïve $CD8^+$ T-cells are stimulated with IL-4 in vitro, they differentiate into IL-4- and IL-5-producing Tc2 cells(126,127). Similar to Th2 cells, Tc2 cell cytokine production is driven by the transcription factors STAT6 and GATA3(8). Tc2 cells, like Th2 cells, stimulate B-cell IgE production, recruit eosinophils, and contribute to allergic responses(128,129).

While effector memory Tc1 cells produce high levels of IFN-γ and cytotoxic granules, Tc2 cells lack these cytotoxic capabilities, rendering them less effective in targeting tumor cells(130). This suggests that converting Tc1 cells to a Tc2 phenotype may undermine the antitumor functions of $CD8^+$ T-cells. In cervical cancer, for instance, tumor cells encourage tumor-infiltrating $CD8^+$ T-cells to acquire a Tc2 phenotype, leading to increased IL-4 and reduced IFN-γ production, which enables tumor immune evasion(131). Similarly, in urothelial bladder cancer, the Tc2-polarized tumor microenvironment contributes to $CD8^+$ T-cell exhaustion and reduced cytotoxicity by decreasing perforin expression, resulting in an exhausted effector memory phenotype(132).

2.4.8 Type 17 cytotoxic T-cells (Tc17)

Tc17 cells are a subset of $CD8^+$ T-cells characterized by IL-17 production and expression of the transcription factors STAT3 and RORγ(133). Researchers debate the specific features of Tc17 cells, with some suggesting that Tc17 cells express T-bet, the transcription factor associated with Th1 and Tc1 cells(134). However, others argue that Tc17 cells differ from Tc1 cells due to their limited cytolytic activity and low expression of granzyme B and perforin(135). Tc17 cells can produce additional cytokines, such as IL-22, GM-CSF, IL-5, and IL-13, depending on the disease context and tissue environment(136,137).

The role of Tc17 cells in the tumor microenvironment remains uncertain. Memory Tc17 cells, with self-renewal and memory-forming capacities, are viewed as potential candidates for cancer immunotherapy(138). Unlike stable Tc17 cells observed post-fungal vaccination, in vitro-generated Tc17 cells can convert to Tc1 cells within tumors, thus serving as a reservoir of Tc1 cells in vivo(138). In contrast, in vivo-generated Tc17 cells maintain a stable phenotype and have been shown to induce Tc1 cell exhaustion, likely by recruiting $CD11b^+Gr\text{-}1^+$ myeloid-derived suppressor cells (MDSCs) in animal studies(139). A specific Tc17 subset, marked by low PD-1 and high OX40 expression, has been linked to poorer patient survival outcomes(135). In hepatitis B infection, IL-17 attracts $CD11b^+Gr\text{-}1^+$ MDSCs, contributing to $CD8^+$ T-cell exhaustion(140). Similarly, in myelodysplastic syndromes, MDSCs are believed to induce $CD8^+$ T-cell exhaustion through the TIM3/Galectin-9 pathway(141).

2.4.9 Regulatory cytotoxic T-cells (Tcreg)

Regulatory T-cells are essential for maintaining immune balance and preventing autoimmune diseases. While $CD4^+Foxp3^+$ cells are widely recognized as the primary regulatory T-cells, numerous studies have shown that $CD8^+$ Tregs also have immunosuppressive roles across various human and murine systems(142-144).

2.4.10 Natural killer T-like cells (NKT-like)

NKT-like cells constitute less than 10% of circulating lymphocytes in adults and display a high-density TCR-CD3 complex, similar to classical T-cells, along with low CD56 expression, typical of cytotoxic natural killer (NK) cells(145). While NKT-like cells are predominantly αβ TCR^+ CD8 T-cells(146), there

are also reports of αβ TCR$^+$ CD4 T-cells(147). Additionally, CD56 expression can be found on NKT, MAIT, and γδ T-cells, resulting in a mixture of conventional and unconventional T-cells within CD56$^+$ T-cell populations(148).

NKT-like cells may contribute to anti-tumor immunity. Their significance has been noted in the prevention and treatment of hepatitis, where liver inflammation and infection are key factors in the development of hepatocellular carcinoma(149,150). Both CD56$^+$ T and NK cells can target HCC cells, but their numbers are often reduced in patient livers, especially in metastatic cases, potentially limiting their anti-tumor effects in vivo(151). In colorectal cancer (CRC), low peripheral levels of NKG2D$^+$ and NCR$^+$ NKT-like cells are observed, while elevated CD16$^+$ NKT-like cells are linked to shorter disease-free survival(152). Similarly, in gastric cancer, a reduced frequency of NKT-like cells expressing activating receptors is associated with diminished anti-tumor activity and shorter survival(153). Intestinal cancers, compared to pancreato-biliary tumors, exhibit higher NKT-like cell infiltration, associated with more favorable outcome(154). Early-stage lung cancer patients show increased circulating NKT-like cells, suggesting potential prognostic value(155). Overall, NKT-like cells may play an important role in cancer prevention and management. However, due to their heterogeneity and tissue-dependent effects, some subpopulations may exert pro-tumor functions. Comprehensive investigation is necessary to distinguish between beneficial and unfavorable prognostic markers, enhancing our understanding of NKT-like cell subpopulations in cancer.

2.5 Role of the T-cells in colorectal cancers

Th1 is well known for robust secretion of IFN-γ and chemokines, facilitating the priming and proliferation of CD8$^+$ T-cell subpopulations(14,15). Furthermore, it has been shown that type 1 T-helper cells (Th1) can enhance Tc1 effector function by targeted delivery of cytokines via acquired pMHC I complexes(13). Numerous studies have shown that a high Th1 presence correlates with favorable prognosis in colorectal cancer(156-161). The role of Th2 and Th17 in the tumor microenvironment of colorectal cancer is more contradictory. Th2 has been found to promote tumor growth in colorectal cancer(16) but also shows anti-tumor activity due to its cytokine secretion profil(17). In terms of patient outcomes, Th2 cells are generally associated with poorer prognosis in colorectal cancer(159,162). Although a high fraction of Th17 was linked to tumor progression due to the promotion of intestinal tumorigenesis(18,19) and angiogenesis by IL-17 expression(20), anticancer functions such as promoting localization of highly cytotoxic CD8$^+$ T-cells to tumor tissues have been also described(21). Although prognostic studies mainly link Th17 cells with negative outcomes(157,161,163-165), this subset is associated with positive prognosis in some specific contexts(21,159,160). Regulatory T-cells (Tregs) mitigate inflammatory damage and may suppress anti-cancer responses at various stages of colorectal cancer progression(22). Prognostic studies indicate heterogeneity within Treg populations: FOXP3 high Tregs or CD25 high FOXP3$^+$ Tregs are linked to poorer outcomes(166,167), while FOXP3 low Tregs or CD30$^+$OX40$^+$CD45RO$^+$ Tregs are

associated with better prognosis(166,168). Additionally, Tfh cells contribute to anti-tumor immunity by supporting tertiary lymphoid structure formation, and their presence correlates with improved outcomes in colorectal cancer(161,169,170).

Microsatellite instability in colorectal cancer is associated with increased infiltration of $CD8^+$ cytotoxic T-cells, particularly type 1 cytotoxic T-cells (Tc1), leading to enhanced tumor cell destruction(8,9). Functional analysis has shown that Type 1 cytotoxic T-cells (Tc1) represent the main component of the terminal-end-route of anticancer immunity by producing high levels of cytolytic cytokines such as perforin, INF-y and granzyme B, thus initiating direct tumor cell killing(8,10), while other cytotoxic T-cell subsets such as type 2 (Tc2)(8,11), or regulatory cytotoxic T-cells (Tcreg)(171) contribute less effectively to tumor cell destruction. A strong Th1/Tc1 response, potentially enhanced by the caspase-1/IL-18 axis, is associated with improved survival in colorectal cancer(172). Although some studies suggest that Tc2 and Tc17 cells may follow Th2 or Th17 pathways (173,174), their exact influence on patient outcomes in colorectal cancer remains unclear.

3. Material and Methods

3.1 Tissue microarray technique

The tissue microarray (TMA) technique, which was developed in 1998 by Kononen, J. et al., makes it possible to simultaneously analyze up to around 600 patients on a single slide(175). This study involves 4 TMA blocks, each consisting of 304 - 612 tumor tissue samples. To prepare a TMA, the various tumor tissue samples from different patients were first fixed in formalin and embedded in paraffin. Samples with a diameter of 0.6 mm were then taken from each donor block (donor) using a hollow needle and placed on a recipient paraffin block (recipient) with pre-punched holes (coordinates). For different research questions, tissue samples of different sizes are punched: for a control cell line TMA (validation of antibodies on transfected cells), 2 mm punches are arranged on the TMA. For immunohistochemistry, 2 mm thin sections were then cut from the recipient paraffin block using a microtome and fixed on a slide. In order to pseudonymize or anonymize the patients, each patient was assigned to a coordinate (Figure 1), given a patient identification number and assigned to the corresponding clinical data in a data file.

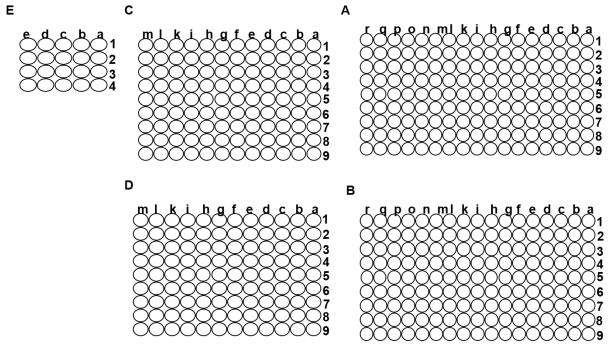

Figure 1: An example of TMA coordinate

3.2 Colorectal cancer tissue microarrays

The study included a total of 1297 colorectal cancers in a tissue microarray (TMA) format with tissue spots measuring 0.6 mm, operated between 2004 and 2019 at the University Medical Center Hamburg- Eppendorf and the Institute of Pathology in the Klinikum Fürth, Fürth, Germany with available data on the expression of MSH2, MSH6, MLH1, and PMS2 leading to the identification of 1203 patients with a microsatellite stable phenotype (MSS) and 94 with a microsatellite instable phenotype (MSI). This cohort was not treated with immune checkpoint inhibitors. Detailed histopathologic data including pathologic tumor stage (pT), pathologic lymph node status (pN), V stage, L stage, RAS mutation or HER2 amplification were available from up to 1286 tumors. All samples came from the archives of the Institutes of Pathology at the University Hospital of Hamburg (Hamburg, Germany) and Institute of Pathology at the Klinikum Fürth, Fürth, Germany. The use of archived remnants of diagnostic tissues for manufacturing of TMAs and their analysis for research purposes, as well as patient data analysis, have been approved by local laws (HmbKHG, x12) and by the local ethics committee (Ethics commission Hamburg, WF-049/09, January 25, 2010). All work has been carried out in compliance with the Helsinki Declaration. A pathologist reviewed every tissue

sample to exclude tissue spots that were lacking cancer cells. Patient characteristics are described in Table 1.

Patients characteristics	No. of patients (%) Total study cohort on TMA (n=1297)
Sex	
Male	351 (27.1%)
Female	264 (20.4%)
Missing data	682 (52.5%)
Macrosatellite status - no. (%)	
Macrosatellite stable (MSS)	1203 (92.8%)
Macrosatellite instable (MSI)	94 (7.2%)
Missing data	0 (0%)
pT stage - no. (%)	
pT1	53 (4.1%)
pT2	268 (20.7%)
pT3	708 (54.6%)
pT4	257 (19.8%)
Missing data	11 (0.8%)
pN stage - no. (%)	
pN-	669 (51.6%)
pN+	605 (46.6%)
Missing data	23 (1.8%)
V stage - no. (%)	
V0	930 (71.7%)
V+	335 (25.8%)
Missing data	32 (2.5%)
L stage - no. (%)	
L0	525 (40.5%)
L1	723 (55.7%)
Missing data	49 (3.8%)
RAS mutation - no. (%)	
Yes	309 (23.8%)
No	401 (30.9%)
Missing data	587 (45.3%)
HER2 amplification - no. (%)	
Positive	17 (1.3%)
Negative	618 (47.6%)
Missing data	662 (51.1%)

Table 1: Patient characteristics shown for 0.6mm TMA.
A single 0.6 mm core represents a colorectal cancer specimen in the cohorts.

3.3 Colorectal cancer large sections

The study included a total of 12 colorectal cancers in a large section format. All 12 cases were inspected by an experienced pathologists to ensure tissue integrity and diagnostic correctness. This cohort was also not treated with immune checkpoint inhibitors. Detailed histopathologic data including pathologic tumor stage (pT), pathologic lymph node status (pN), V stage, L stage, RAS mutation or HER2 amplification were available from all 12 tumors. All samples came from the archives of the Institutes of Pathology at the University Hospital of Hamburg (Hamburg, Germany) and Institute of Pathology at the Klinikum Fürth, Fürth, Germany. The use of archived remnants of diagnostic tissues for manufacturing of large sections and their analysis for research purposes, as well as patient data analysis, have been approved by local laws (HmbKHG, x12) and by the local ethics committee (Ethics commission Hamburg, WF-049/09, January 25, 2010). All work has been carried out in compliance with the Helsinki Declaration. Patient characteristics are described in Table 2.

Patients characteristics	No. of patients (%) **Total study cohort on large sections (n=12)**
Sex	
Male	0 (0%)
Female	0 (0%)
Missing data	12 (100%)
Macrosatellite status - no. (%)	
Macrosatellite stable (MSS)	6 (50%)
Macrosatellite instable (MSI)	6 (50%)
Missing data	0 (0%)
pT stage - no. (%)	
pT1	0 (0%)
pT2	1 (8.3%)
pT3	7 (58.3%)
pT4	4 (33.4%)
Missing data	0 (0%)
pN stage - no. (%)	
pN-	6 (50%)
pN+	6 (50%)
Missing data	0 (0%)
V stage - no. (%)	
V0	11 (91.7%)
V+	1 (8.3%)
Missing data	0 (0%)
L stage - no. (%)	
L0	8 (66.7%)
L1	4 (33.3%)
Missing data	0 (0%)
RAS mutation - no. (%)	
Yes	2 (16.7%)
No	8 (66.7%)
Missing data	2 (16.6%)
HER2 amplification - no. (%)	
Positive	0 (0%)
Negative	10 (83.3%)
Missing data	2 (16.7%)

Table 2: Patients characteristics large section

3.4 Immunohistochemical staining

We used our recently developed BLEACH&STAIN(176) multiplex fluorescence approach that enables the analysis of 19 biomarkers in paraffin embedded and formalin fixed tissue to identify a localization-specific relationship between leukocytes, tumor cells and vessels in the tumor microenvironment. The method of immunohistochemistry in bright field and multiplex fluorescence and the principle of staining with opal fluorophores included here are described in detail below.

3.4.1 Bright-field immunohistochemistry (hfIHC)

The samples on the slide were first incubated overnight at 60 °C in an incubator to deparaffinize them. They were then incubated in xylene for 3 x 10 min, followed by rehydration through a descending ethanol series (99 %-, 96 %-, 80 %-$H_2O_{dest.}$). The tissue was autoclaved at 2 bar and 121 °C for 1.5 h. After an initial wash of the sections with TBS/T buffer for 5 min, they were blocked with peroxidase for 10 min and the primary antibody was applied. For each antibody, the optimal dilution and pH value was previously determined according to the International Working Group for the Validation of Antibodies (IWGAV)(177,178). The tissue sections were incubated with the primary antibody for 1 hour at 37 °C in an incubator, then washed for 2 x 5 minutes with TBS/T buffer, and incubated with the corresponding secondary antibody for 30 minutes at 37 °C. After another wash (2 x 5 minutes with TBS/T buffer), the samples were stained for 10 min with 3,3'- Diaminobenzidine (DAB), a chromogen that produces a brown color when reacting with peroxidase. Finally, hematoxylin staining was performed to visualize the nucleus (blue). Sections were blued with tap water for 5 min to remove excess hematoxylin, dehydrated through an ascending alcohol series, followed by xylene, and fixed. After coverslipping the sections with a Tissue-Tek Film coverslipping machine from Sakura, the slides were ready for further microscopic examination.

3.4.2 Multiplex fluorescence immunohistochemistry

In contrast to the consecutive examination of different antibodies in bright field, the method of multiplex fluorescence immunohistochemistry was employed to examine multiple antibodies simultaneously on the same cell (Table 3). For this purpose, tissue sections of 4 µm thickness were prepared for staining. The paraffin was removed from the tissue overnight at 60 °C in an incubator. To unmask the proteins in the tissue, the sections were first deparaffinized. Subsequently, the tissue was incubated for 10 min in 10 % formalin, washed with $H_2O_{dest.}$, and the cuvette was filled with the buffer determined for the respective antibody. The tissue was then autoclaved for 1.5 h at 2 bar and 121 °C. In the subsequent immunohistochemical staining processes, the tissue sections were each stained with 4 different primary antibodies, followed by a counterstaining with 2-phenylindole diamidine (DAPI). The dilutions of the antibody were determined individually before each staining and consequently calculated for a final volume of 300 µl, using an "Antibody Diluent Block" (blocking buffer) to minimize endogenous peroxidase activity and thus reduce non-specific binding of proteins with hydrogen peroxide, thereby limiting background staining. The tissue samples were incubated for

10 min in blocking buffer in a humidity chamber. The blocking buffer was then removed, 300 µl of the diluted antibody was applied and incubated for 30 min in the humidity chamber at room temperature. After a wash with TBS/T buffer for 3 x 2 min, the sections were incubated with horseradish peroxidase (HRP)-conjugated secondary antibody for 10 min and then rinsed again with TBS/T buffer for 3 x 2 min. The multiplex fluorescence immunohistochemistry offers various techniques, including tyramide signal amplification (TSA). By using this opal signal amplification technique during multiplex fluorescence immunohistochemical staining, it is possible to remove the dye from the tissue and re-stain the tissue. This means that less sample material is required from the patient and the tissue can be used several times and analyzed in different ways. The respective fluorophore opal (Akoya Bioscience) was diluted in DMSO according to the product description. These were then applied to the tissue at a 1:100 dilution with Amplification Diluent (Akoya Bioscience) and incubated for 10 min at room temperature in a humidity chamber. After rinsing with TBS/T buffer for 3 x 2 min, the tissue was incubated in pH 6, pH9 buffer in the microwave at 1,000 watts for 5 min. The samples were then heated at 1,000 watts for 5 min and at 270 watts for another 5 min. These steps were repeated for all required antibodies and opals (Table 3). The nuclei of the tissue were counterstained with DAPI and coverslipped. The fluorescence dyes OPAL 520 (Cat. #FP1487001KT AKOYA Biosciences, Menlo Park, California, United States), OPAL 570 (Cat. #FP1488001KT, AKOYA Biosciences), OPAL 620 (Cat. #FP1495001KT, AKOYA Biosciences), and OPAL 690 (Cat. #FP1497001KT, AKOYA Biosciences) were used for visualization of antibody binding. Details on antibody dilutions, antibody retrieval procedures and OPAL dyes are given in Table 3. Digital images of mfIHC slides were acquired with a Leica Aperio VERSA 8 automated epifluorescence microscope and AKOYA's PhenoImagerTM HT slide scanner.

Antibody target	Identifier	AR (pH value)	Dilution	Staining position	Opal dye	BLEACH&STAIN
RoRγT	Millipore, Clone: 6F3.1 Cat#: MABF81	7.8	1:450	1	520	Cycle 1
TIM-3	MSVA, Clone: MSVA-366R Cat#: SKU: 3484-366R-01	7.8	1:100	2	570	Cycle 1
GATA3	MSVA, Clone: MSVA-550R Cat#: 3209-550R-01	7.8	1:75	3	620	Cycle 1
T-bet	Epitomics, Clone: EP263 Cat#: AC-0240A	9.0	1:150	4	690	Cycle 1
CTLA-4	MSVA, Clone: MSVA-152R Cat#: SKU: 3451-152R-01	9.0	1:100	5	520	Cycle 2
PD-1	abcam, Clone: [EPR4877(2)] Cat#: ab137132	9.0	1:450	6	570	Cycle 2
CD56	MSVA, Clone: MSVA-056R Cat#: SKU: 6173-056R-01	9.0	1:150	7	620	Cycle 2
GranzymB	Leica, Clone: 11F1 Cat#: NCL-L-GRAN-B	9.0	1:50	8	690	Cycle 2
CD27	MSVA, Clone: MSVA-027M Cat#: SKU: 2503-027M-01	9.0	1:450	9	520	Cycle 3
CD3	DAKO, Clone: CD3 Cat#: IR503	9.0	1:3	10	570	Cycle 3
BCL6	DAKO, Clone: PG-B6p Cat#: IR625	9.0	RTU	11	620	Cycle 3
CD11c	abcam, Clone: [EP[347Y] Cat#: ab52632	9.0	1:1000	12	690	Cycle 3
FOXP3	BioLegend, Clone: 206D Cat#: 320102	9.0	1:75	13	520	Cycle 4
CD4	MSVA, Clone: MSVA-004R Cat#: SKU: 2278-004R-01	9.0	1:150	14	570	Cycle 4
CD8	DAKO, Clone: C8/144B Cat#: IR623	9.0	1:25	15	690	Cycle 4
panCK	MSVA, Clone: MSVA-000R Cat#: SKU: 2105-000R-01	9.0	1:600	16	520	Cycle 5
Ki67	MSVA, Clone: MSVA-267M Cat#: SKU: 2082-267M-01	9.0	1:150	17	570	Cycle 5
HLA-DR	MSVA, Clone: MSVA-470R Cat#: SKU: 3328-470R-01	9.0	1:150	18	620	Cycle 5
CD31	MSVA, Clone: MSVA-031M Cat#: SKU: 2517-031M-01	9.0	1:250	19	690	Cycle 5

(MSVA: MS Validated Antibodies GmbH, AR: antigen retrieval)

Table 3: List of the used antibodies, antigen retrieval (AR), dilutions, and Opal dyes for multiplex fluorescence immunohistochemistry.

3.5 BLEACH&STAIN Framework

To perform sequential 4+1 marker multiplex fluorescence immunohistochemistry staining on the same section, it is essential to completely and gently remove the previous staining from the tissue, thereby reducing the residual intensity of the fluorochromes to background levels. The particular challenge of an efficient bleaching process is to minimize tissue damage so that many additional rounds of staining can be carried out. The BLEACH&STAIN process developed in this work combines the complete, tissue-friendly and rapid removal of the bound antibodies by cooling the tissue to 4 °C, incubating it in hydrogen peroxide and irradiating it with 1,600 W. For this purpose, the tissue was applied to specially coated slides with excellent adhesion before the first staining (X-TRA-SLIDES, Leica Biosystems). To gently remove the coverslips after the first staining, the slides were placed in

buffer (pH 7) overnight. Hydrogen peroxide was freshly prepared before each experiment. A glass tank was covered with reflector foil to enhance the effect of bleaching by the light radiation. The glass tank was placed in a container with water and ice (4 - 5 °C). The slides were rinsed in H_2O_{dest}, placed in the glass tank and covered with H_2O_2. A 1,600 watt lamp was placed approx. 60 cm away from the glass tank and the slides were bleached for 4 hours. The H_2O_2 was replaced with fresh H_2O_2 every hour. The emission of the antibody was measured under the microscope after 4 h, and the experiment was stopped at an emission of 150 nm to protect the tissue. The slides were rinsed in $H_2O_{dest.}$ and treated in the microwave for re-staining. The bleaching process was stopped as soon as the fluorescence signal of all fluorochromes was vanished (exposure time > 600ms). Finally, the four sequential digital images were aligned and thus merged into a single 19+1 mfIHC image using a custom software written in the Python program language(179). The detailed BLEACH&STAIN approach is shown in Figure 2 A-B.

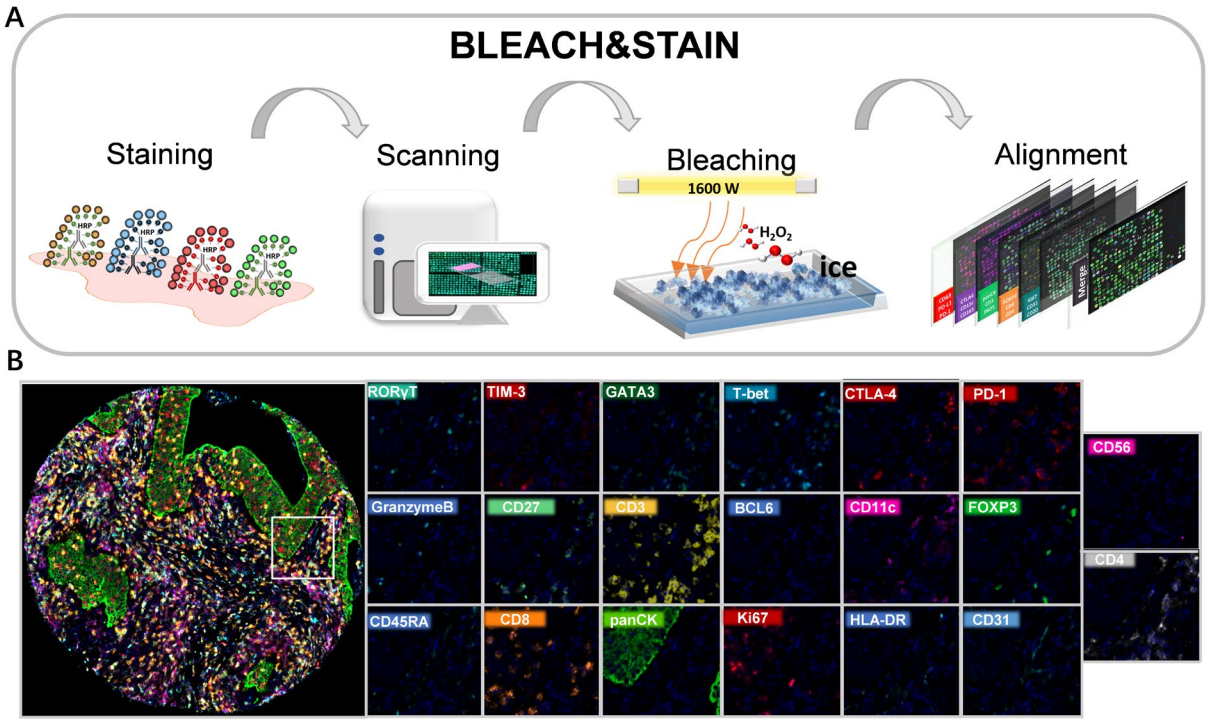

Figure 2: BLEACH&STAIN framework
(A-B) The previously described BLEACH&STAIN multiplex fluorescence immunohistochemistry technology facilitates high throughput analysis of 20 antibodies that were stained in 5 sequential staining cycles (see Table 3).

3.6 Deep learning-based framework for automated 19-plex BLEACH&STAIN mfIHC image analysis

Image analysis was performed using the previously trained(176,180) deep learning-based (U-Net) framework for cell detection, cell segmentation, intensity measurement of the used fluorophores (range 0-255, i.e., a continuous numerical value indicating the fluorescence signal strength), processing of intensity values, cell distance, and cell-to-cell interaction analysis using Python version 3.8(179) (RRID:SCR_008394), R version 3.6.1 (RRID:SCR_001905, The R foundation)(181) and the Visiopharm software package (RRID:SCR_021711, Hoersholm, Denmark).

1. The TMAs were segmented and a previously trained(176) DeepLabv3+ was used to quantify the area of every individual TMA spot and large section regions (i.e., each patient).

2. To identify individual cells (i.e., cell segmentation) a previously trained deep learning-based (U-Net) framework for segmentation of cell nuclei and the adjacent cytoplasm was used(180). Thus, the intensity of the used fluorophores (range 0-255, i.e., a continuous numerical value indicating the fluorescence signal strength) in the nuclear and cytoplasmic cell compartment, as well as the localization of every cell, were documented in per-cell data.

3. Marker positivity (i.e., CD3, CD8, CD4, FOXP3, T-bet, GATA3, RORγT, BCL6, CD27, CD56, CD11c, TIM-3, PD-1, CTLA-4, panCK, Ki67, CD31, GranzymeB, HLA-DR, CD45RA) was evaluated by a deep-learning (U-Net) system for every marker individually that classified the marker either positive or negative based on multiple features which have been identified by the convolutional neural network within the training set (e.g., the intensity level, distribution of the marker intensity across the cell, and cell shape). The individual thresholds were used to label the initial training set, which was manually corrected as needed and used to train "provisional" deep learning systems to continuously expand the training set and improve the accuracy of the deep learning system(180). The final deep learning system (U-Net) for marker positivity was trained on 250 tissue samples using the deep-learning frameworks Keras and Tensorflow (RRID: SCR_016345, in Python version 3.87) and the Visiopharm software package.

4. For identification and definition of immune cell subpopulations unsupervised X-shift clustering was applied and revealed 242 subpopulations (Figure 3A-B). Within these subpopulations, the well-characterized expression profile of Tc1 ($CD3^+CD8^+$T-bet^+), Th1 ($CD3^+CD4^+$T-bet^+), Tc2 ($CD3^+CD8^+GATA3^+$), Th2 ($CD3^+CD4^+GATA3^+$), Tc17 ($CD3^+CD8^+$ $ROR\gamma T^+$), Th17 ($CD3^+CD4^+ROR\gamma T^+$), Tcreg ($CD3^+CD8^+FOXP3^+$), Treg ($CD3^+CD4^+FOXP3^+$), Tfh ($CD3^+CD4^+BCL6^+$), NKT-like ($CD3^+CD56^+$), dendritic cells ($CD11c^+$), and tumor cells ($panCK^+$) was identified. These 12 main subsets were further subclassified in 45 T-cell subpopulations and 9 other immune cells as well as tumor cell subpopulations according to their functional state (proliferation, cytotoxicity, immune checkpoint expression, Figure 3C). The detailed image analysis has been described in detail earlier(180,182,183).

5. The per-cell data derived from the image analysis framework represent the input data to assess spatial interactions (cell-to-cell contact), cell distances (µm), T-cell densities (cells/mm^2), T-cell composition (%), fraction of functional marker positive cells (%) and T-cell accumulation.

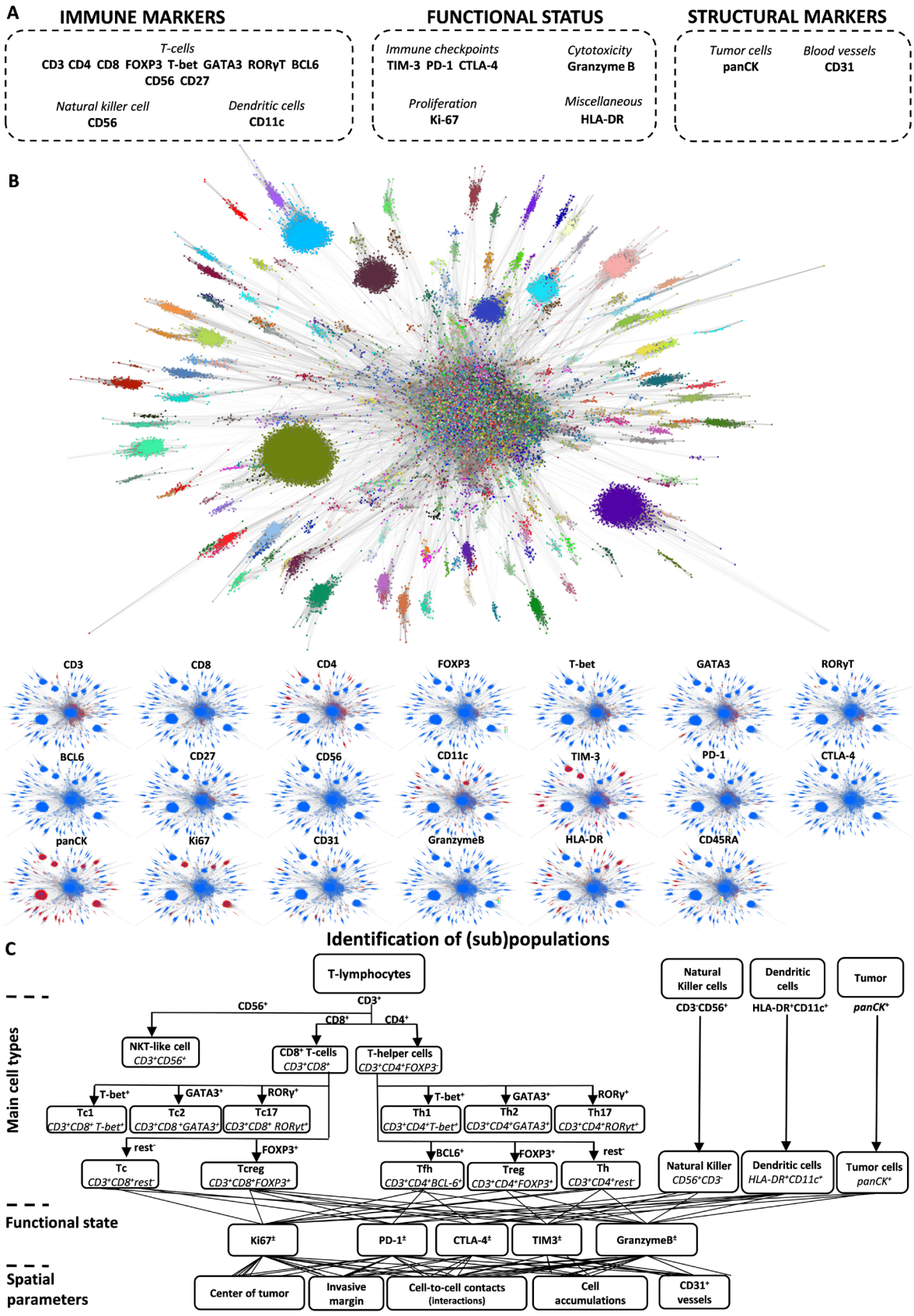

Figure 3: Identification of cell subpopulations.
(A) Organizational grouping of the used 19 markers into three groups.
(B) Unsupervised X-shift clustering identified 242 immune cell subpopulations.
(C) The expression profile that is used to identify 54 immune and tumor cell subpopulations according to the cell type and its functional state.

3.6.1 TMA analysis

For TMA analysis, spots were manually segmented using the Visiopharm software package (Hoersholm, Denmark). Six parameters were measured for every TMA core:

1. The density of each measured T-cell subpopulation per square millimeter was calculated by dividing the number of the T-cell by the measured area of each tissue spot. the area of every individual TMA spot was produced by a previously trained DeepLabv3+(183).

2. The composition of each T-cell subpopulation was calculated by dividing the number of the specific T-cell subset (e.g., Tc1) by the total number of T-cells.

3. The fraction of (functional) marker positive T-cell subpopulation was calculated by dividing the number of marker positive T-cells of this specific subset (e.g., $TIM3^{+}$Tc1) by the total number of T-cells belonging to the same distinct phenotype (e.g., Tc1)(183).

4. The relative intensity of the functional marker including immune checkpoint TIM3, PD-1, CTLA-4, cytotoxicity marker GranzymeB, and proliferation marker Ki67 was calculated by dividing the raw intensity values by the mean intensity of the relative marker on all this specific marker positive cells in the whole TMA slide.

5. Parameters reflecting cell-to-cell contacts, including (p)-normalized interactions and normalized interactions, were calculated to assess cellular interactions within the TMA spots. Detailed methodologies for these calculations are provided in the subsequent section, "Spatial Analysis."

3.6.2 Large section analysis

To validate the findings from the TMA analysis and compare the underlying changes of T-cell composition in MSI patients between different large section compartments, the center of the tumor and the invasive margin were manually annotated in each large section. Subsequently, each compartment (invasive margin and tumor center) was evenly divided into eight distinct regions to obtain adequate samples for comparative analysis.

1. The center of the tumor and invasive margin were defined for 12 large sections. Two experienced pathologists, trained according to standardized criteria, annotated the invasive margin and the tumor center. Initially, a boundary line was drawn at the interface between the stroma and the tumor. The invasive margin was delineated as a region extending 360 μm into the stromal tissue and 360 μm into the tumor from this boundary. The tumor center was defined as the tumor parenchyma located away from the boundary line(184).

2. T-cell densities (cells/mm2), T-cell composition (%), fraction of functional marker positive T-cells (%) and parameters reflecting cell-to-cell contacts were measured for every tissue compartment.

3.7 Spatial analysis

3.7.1 Cell-to-cell contacts

A cell-to-cell contact was defined as the distance of eight or fewer micrometers between the center points of two cells as described in our previous study(180,182,183). R version 3.6.1 (The R foundation) was used to calculate the nearest distance between every cell subpopulation. The proportion of normalized interactions "(p)-normalized interactions" was calculated by dividing the number of cell-to-cell contacts of two interacting immune cell subpopulations by the overall number of cell-to-cell contacts of all analyzed immune cells. The "normalized interactions" were calculated by dividing the number of cell-to-cell contacts of two interacting immune cell subpopulations by the number of cells in these two immune cell subpopulations. The number of random relative interactions (noise) was calculated by measuring the number of all cell-to-cell contacts per area and used to estimate whether the relative cell-to-cell counts of the immune cell subpopulations were significantly enriched –compared to the random "background" interactions – or just by chance.

3.7.2 Nest analysis

Dense accumulations of T-cells, accompanied by an increase in cell-to-cell contacts, were identified as T-cell nests (Figure 4 A-E). DBSCAN algorithm (R "dbscan" package, R "opticskxi" package) was used to identify the T-cell accumulation. MinPts was set as 27 to define the minimum number of cells in a T-cell nest (Figure 4 A-B). Eps was identified by running the DBSCAN algorithm in different eps values on manually selected T-cell accumulation (Figure 4 C-D). The crossing point between the sensitivity and specificity curves showing the optimal eps that was found as 40 (Figure 4 C).

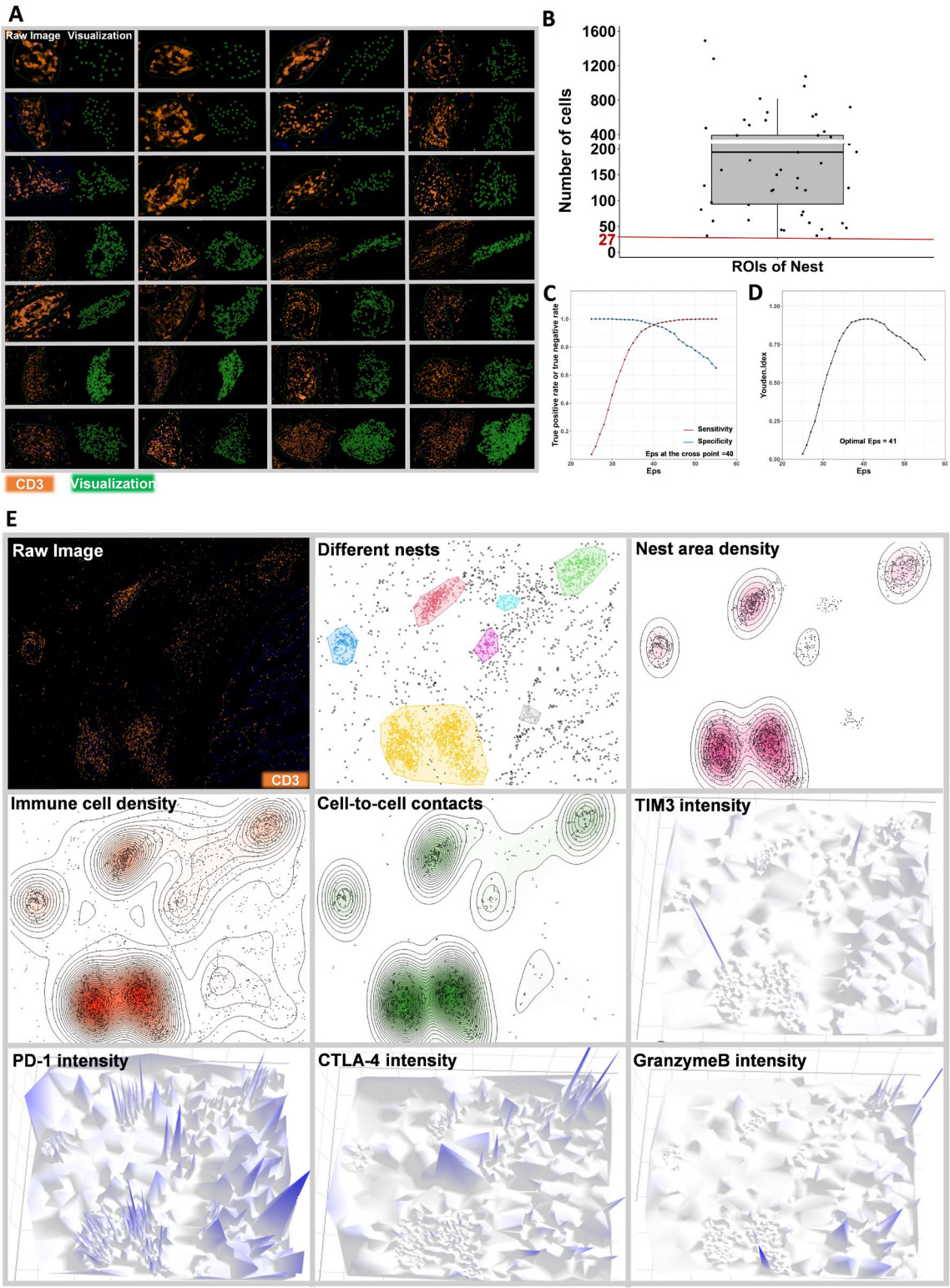

Figure 4: Nest detection

(A) Representative images and T-cell visualization showing manually selected regions of the nest.
(B) Box plot showing the number of cells in 60 different nest regions. The red line represents the minimum number of cells is 27.
(C) Specificity and sensitivity curves showing the accuracy of nest detection based on a range of Eps from 25 to 55. The Eps at the cross point is 40.
(D) Youden's Index curve showing the accuracy of nest detection based on a range of Eps from 25 to 55. The Eps at optimal Youden's index is 41.
(E) Representative images showing nests detected by the DBSCAN algorithm with optimal parameters. The immune cell density, cell-to-cell contacts, and functional marker intensity in the nest area are performed.

3.8 Statistical analysis

Statistical calculations were performed with R version 3.6.1 (The R foundation) (181,185) and JMP Pro 17 software package (SAS Institute Inc., NC, USA)(186). The clinical and histopathological parameters of the patients were reported as counts and percentages for categorical data and compared using pearson's chi-square tests. All continuous variables in different groups were compared using analysis of variance (JMP Pro 17 software package or R “stats” package). Immune parameters between groups were compared using a t-test. In the case of large section analysis, the regions were randomly separated into 48 regions for comparison and heterogeneity analysis. Unsupervised X-shift Clustering(187) was applied to differentiate patient subgroups based on their marker expression pattern (“VorteX” software). The clustering via X-shift was performed using the “number of nearest neighbors” (K) method and the optimal value for K (20) was determined via elbow points and resulted in 242 clusters. All ratios with a denominator of zero were treated as having no value as well as being excluded from the analysis. All p-values were two-sided, and p-values <0.05 were considered as significant.

3.8.1 X-Shift-Clustering

Accurate identification of cell populations is crucial for multidimensional single-cell analysis of the tumor microenvironment. In this study, X-shift clustering was employed to identify and delineate biologically relevant phenotypes and subpopulations within the single-cell dataset (VorteX.jar, Java™ Platform)(187). The X-shift algorithm organizes complex datasets into 2- or 3-dimensional graphs using weighted K-nearest neighbor density estimation (KNN-DE), which incorporates nearest neighbor classification and probability density function estimation. Following graph construction, the density of individual cell events is utilized to organize the data into clusters. Thus, 242 subpopulations could be differentiated in this study.

4. Results

4.1 Technical aspects

A total of 1112 (85.7 %) of 1297 human colorectal cancer tissue samples in the 0.6 mm (tissue cores in diameter) tissue microarray (TMA) format were interpretable in this study (Figure 5). The remaining 185 tumor samples were excluded due to the complete loss of tissue spots or the lack of unequivocal cancer cells. Representative images of an MSI and MSS T-cell immune tumor microenvironment are shown in Figure 6.

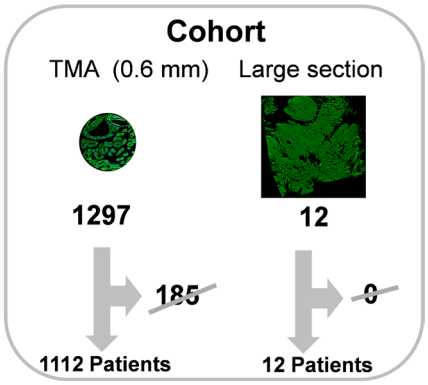

Figure 5: Cohort
(A) 1112 (85.7 %) of 1297 human colorectal cancer tissue samples in the 0.6 mm (tissue cores in diameter) tissue microarray (TMA) format and 12 (100 %) of 12 patients in a large section format were analyzed in the study. For detailed patient characteristics see Table 1-2.

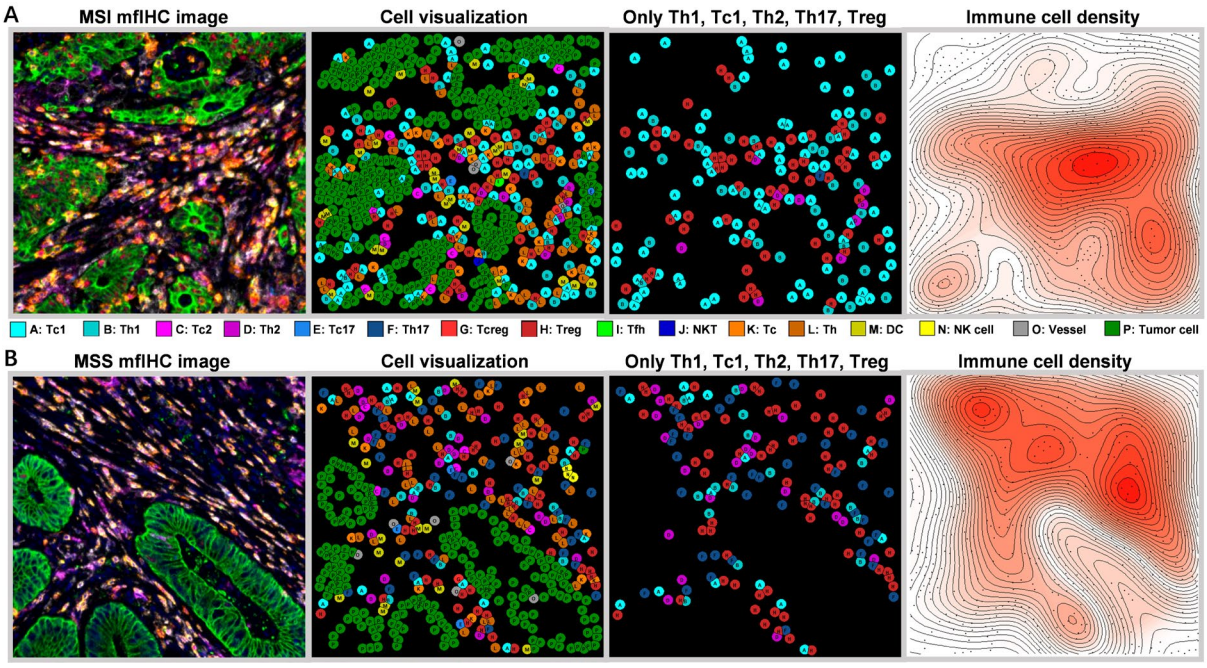

Figure 6: Representative images
(A-B) Representative images of an MSI (A) and MSS (B) T-cell immune tumor microenvironment and its visualization through artificial intelligence-based image analysis.

4.2 Density and composition between MSI and MSS

Although the abundance (i.e. density in cells/ mm^2) of most T-cell subpopulations was significantly higher in 73 microsatellite instable (1628±1687, MSI) compared to 1039 microsatellite stable (1028±1113, MSS) colorectal cancers ($p<0.05$ each), the fraction of Type 1 (T-bet$^+$), Type 2 (GATA3$^+$), Type 17 (RORγT$^+$), regulatory (FOXP3$^+$), and follicular (BCL6$^+$) cytotoxic (CD3$^+$CD8$^+$) or

helper ($CD3^+CD4^+$) T-cells showed marked differences between MSI and MSS patients (Figure 7A-B). For instance, the fraction of Tc1 and Th1 as well as other cytotoxic T-cells was significantly enriched in MSI patients ($p<0.001$ each), while the fraction of Th2, Th17, Tregs and other T-helper cells ($p<0.05$ each) was significantly higher in MSS colorectal cancers (Figure 7A-B). The strongest difference was seen between MSI and MSS colorectal cancers for the dramatically enriched fraction of Tc1 in MSI patients (Figure 7C).

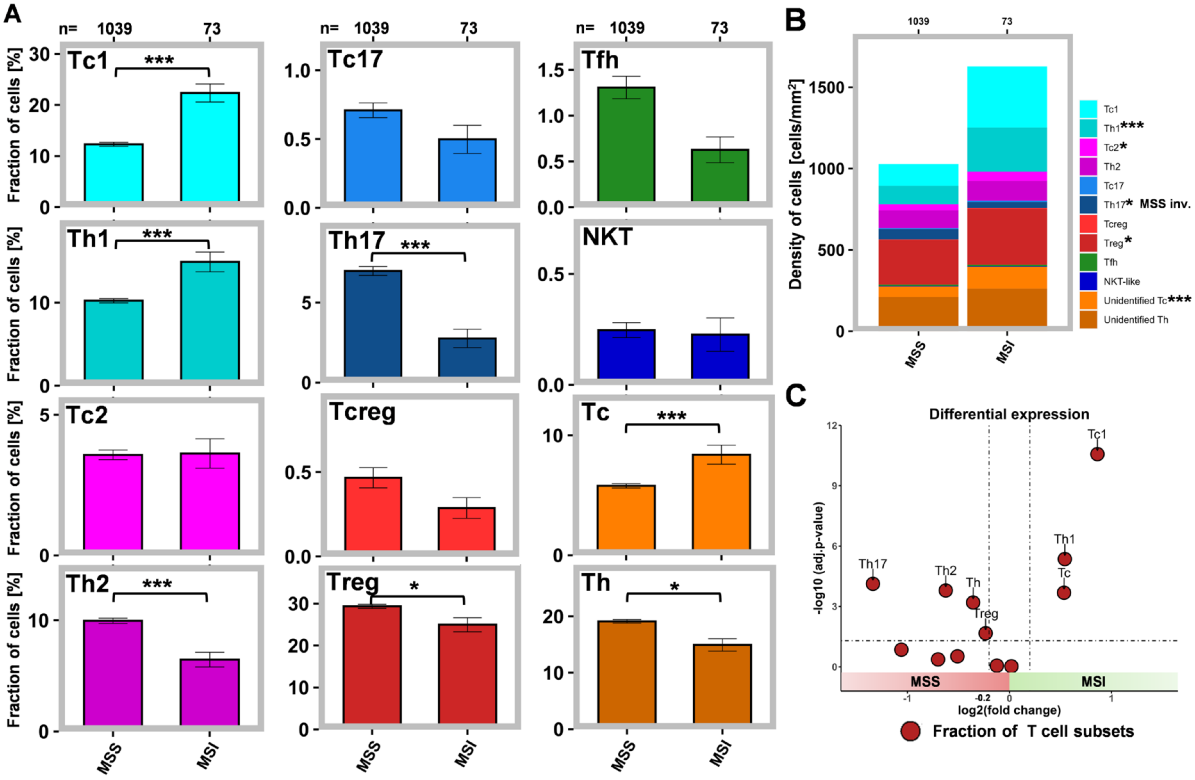

Figure 7: Fraction and density of T-cell subsets between MSS and MSI colorectal cancers
(A) The fraction (%) of T-cell subsets is shown between MSS and MSI colorectal cancers. The error bars indicate the standard error of the mean of each fraction. *p<0.05, **p<0.01, and ***p<0.001.
(B) The total cell density (cells/mm^2) of T-cell subpopulations is shown between MSS and MSI colorectal cancers. ***p<0.001.
(C) Volcano plot depicting log^2-fold change on the x-axis and $-log^{10}$ adjusted p-values on the y-axis of fraction (%) of T-cell subsets in MSI patients compared to MSS patients.

4.3 Functional marker expression in MSI and MSS

The fraction of TIM3 expressing cells was significantly higher in MSI patients compared to MSS in almost all analyzed cytotoxic and helper T-cell subpopulations ($p<0.05$, Figure 8A). A significantly higher fraction of CTLA-4 expression in MSI was found for Th1, Th17 and Tregs ($p<0.01$, Figure 8B), while increased PD-1 expression in MSI was seen in both Tc1 and Th1 cells ($p<0.01$, Figure 8C). An increased fraction of Granzyme B positive cells was detected only for Tc17 ($p<0.05$, Figure 8D). The proliferation rate was found to be increased for Tc1, Tc2, and Tc17 in MSI compared to MSS ($p<0.05$ each, Figure 8E).

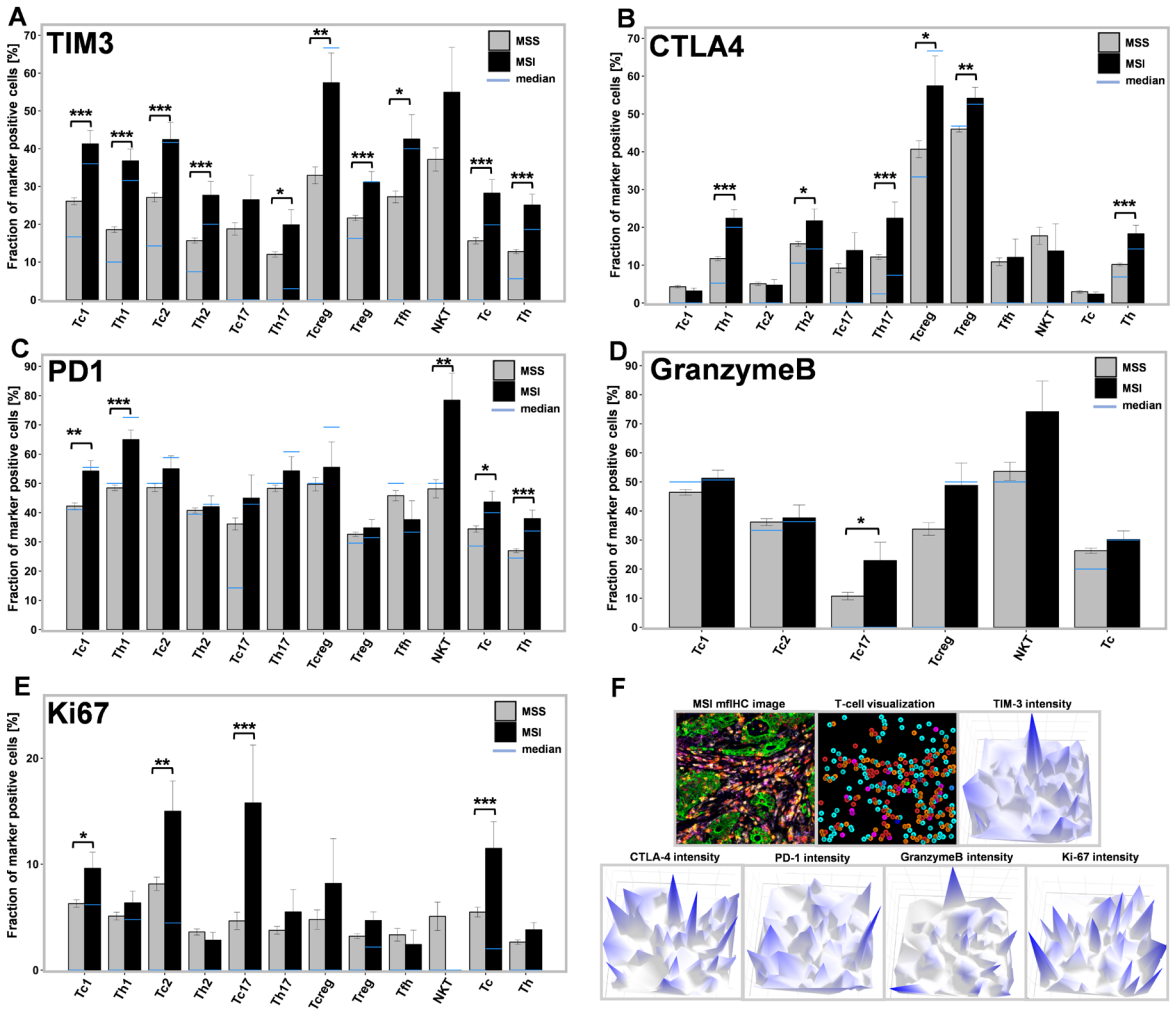

Figure 8: Functional markers between MSI and MSS

(A-E) Fraction (%) of marker positive cells is shown for each T-cell subpopulation between MSI (black and MSS (grey) patients. The blue segments inside or outside the bars indicate the median value of each fraction. The error bars indicate the standard error of the mean of each fraction. *p<0.05, **p<0.01, and ***p<0.001.

(F) Representative images showing the functional marker expression in the tumor microenvironment of MSI patients.

4.4 Spatial interplay between MSI and MSS

The comparison of relative cell-to-cell contacts ((p)-normalized cell interactions) between MSI and MSS patients revealed a markedly increased interaction between Th1 and Tc1 as well as dendritic cells and Tc1 cells in MSI patients (p<0.001, Figure 9A). The spatial orchestration in MSS patients was characterized by the strongest (p)-normalized interactions between Th17 and Tregs as well as dendritic cells (p<0.05, Figure 9A). Of note, a significant normalized interaction (i.e., significant interactions compared to the background of random interactions) between Tc1 and Th1 was exclusively seen in MSI patients but was absent in MSS patients (p<0.001, Figure 9 C-D). A significant normalized interaction between Tregs and Th17 was exclusively detected in MSS

patients (p<0.001, Figure 9 C-D).

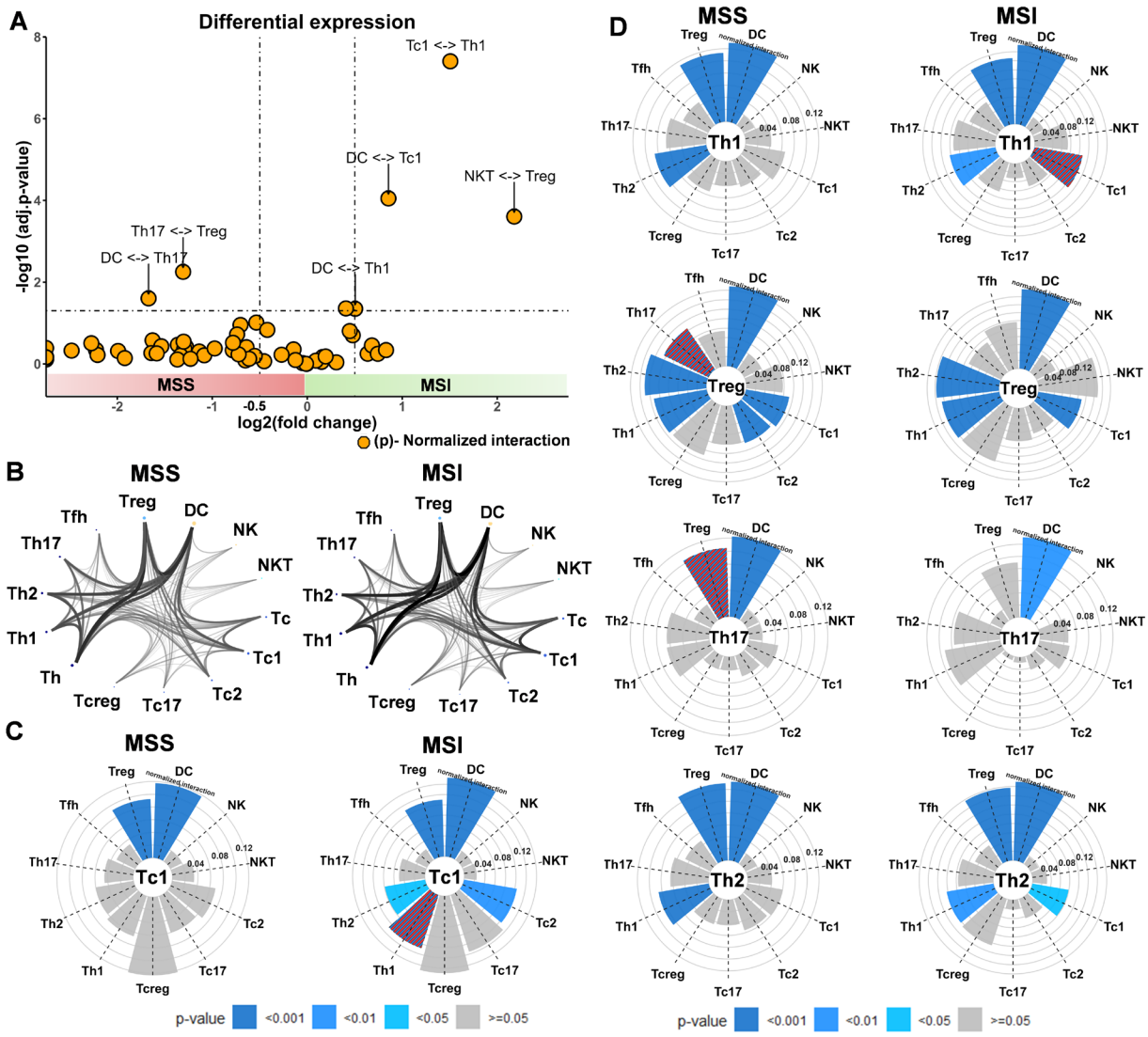

Figure 9: Cell-to-cell interactions between MSI and MSS

(A) Volcano plot depicting log^2-fold change on the x-axis and $-log^{10}$ adjusted p-values on the y-axis of (p) normalized cell-to-cell interactions of T-cell subsets, dendritic cells and natural killer cells in MSI patients versus MSS patients.

(B) Profile of normalized cell-to-cell interactions of T-cell subsets, dendritic cells and natural killer cells in MSI patients versus MSS patients. The thickness of the connections in the cord plots correlates with the number of relative cell interactions, and the size of the nodes indicates the number of cells per cell subpopulation.

(C-D) Circular bar plots indicate the significance of normalized cell-to-cell interactions compared to the background noise (size, shades of blue and grey) and the significant differences between MSS and MSI are highlighted in red.

4.5 Large sections validation and CT vs. IM.

The additional analysis of 12 large sections of 6 MSI and 6 MSS colorectal cancers confirmed the characteristic immune phenotype of MSI colorectal cancers (Figure 10 A-B) and the increased level of immune checkpoint expression in MSI patients in the center of the tumor (Figure 11). The comparison of (p)-normalized interactions also confirmed dramatically increased interaction

between Th1 and Tc1 ($p<0.05$, Figure 10C) as well as dendritic cells and Tc1 cells ($p<0.001$, Figure 10C) in MSI patients compared to MSS patients in the center of the tumor. However, the characteristic composition and interactions of T-cell subpopulations found in the center of the tumor in both the TMA and the large section cohort were not found at the invasive margin (Figure 7, 10A-B). Additional T-cell nest analysis identified enrichment of the fraction of Tc1 ($p<0.001$, Figure 10D) located in T-cell nests of the center of the tumor but not at the invasive margin of MSI patients compared to MSS patients (Figure 10D).

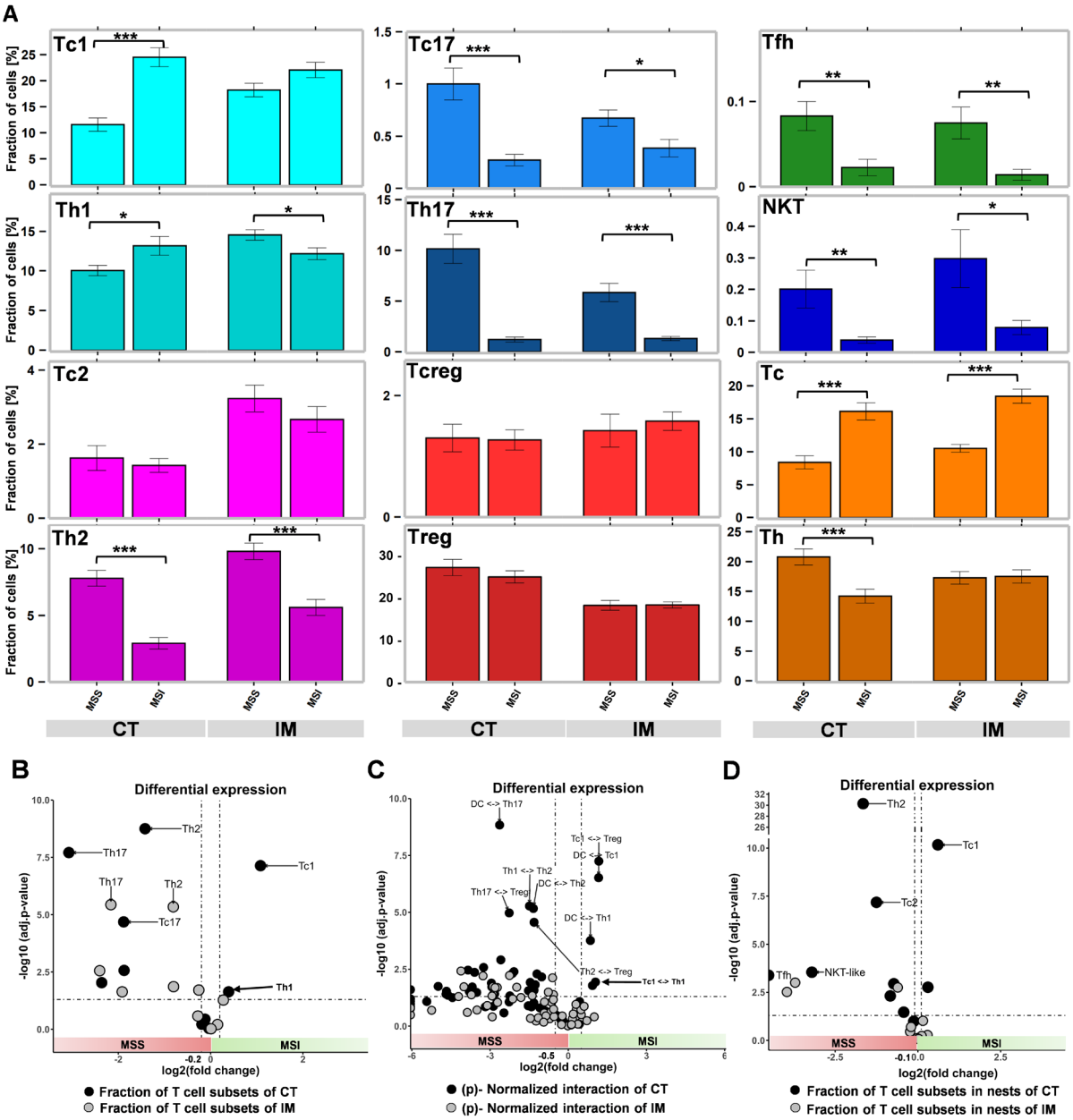

Figure 10: Large section validation and difference between MSI and MSS patients in CT versus IM
(A) The fraction (%) of T-cell subsets is shown between MSS and MSI colorectal cancers in both the center of the tumor (CT) and at the invasive margin (IM) across 12 large sections. The error bars indicate the standard error of the mean of each fraction. *p<0.05, **p<0.01, and ***p<0.001. (B-D) Volcano plot depicting $\log^2$-fold change on the x-axis and $-\log^{10}$ adjusted p-values on the y-axis of T-cell fraction (B), (p)-normalized cell-to-cell interactions (C), and the fraction of T-cell subsets in T-cell nests (D) between MSI and MSS patients.

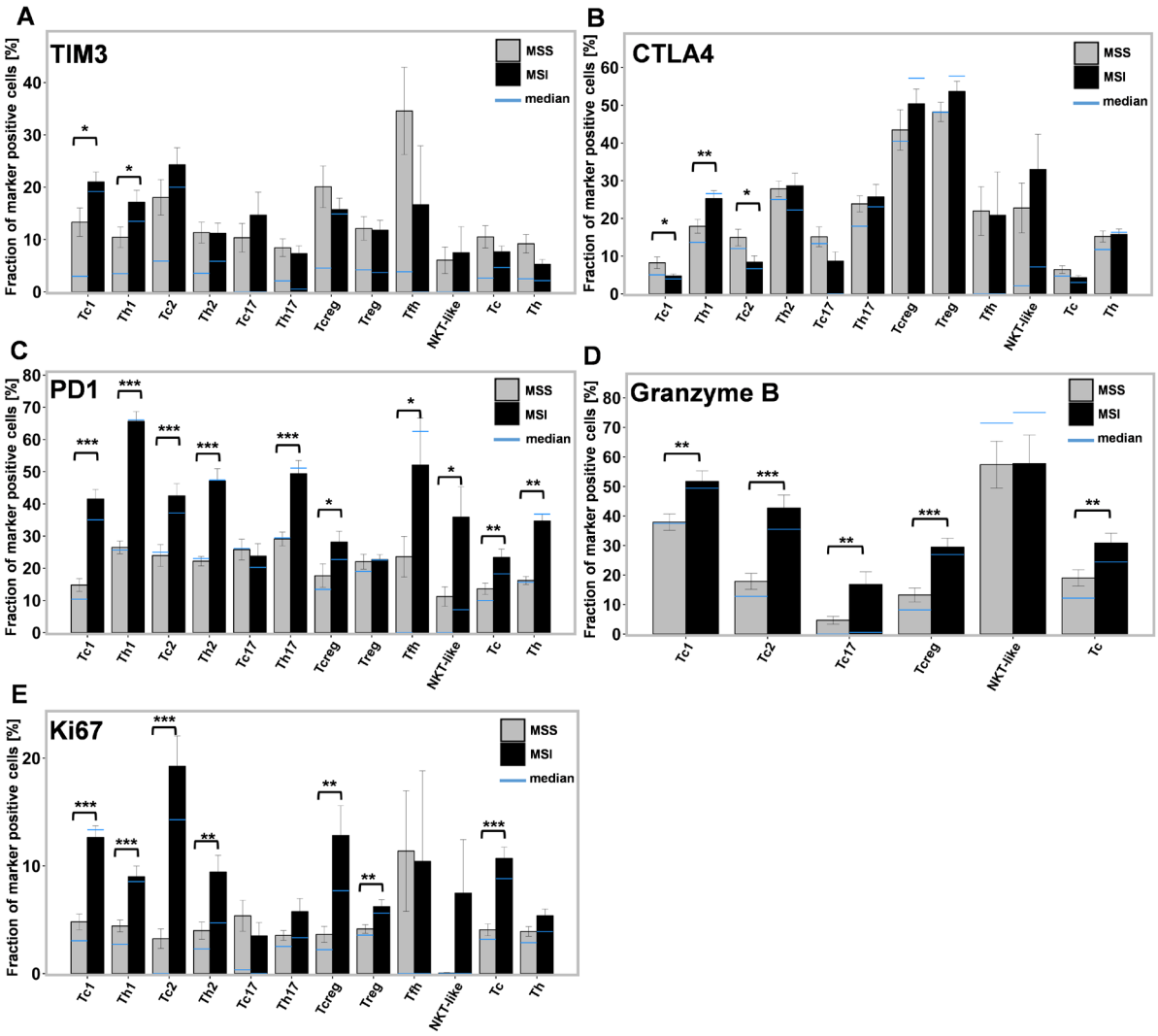

Figure 11: Functional markers between MSI and MSS in the center of tumor of large sections
(A-E) Fraction (%) of marker positive cells is shown for each T-cell subset between MSI (black) and MSS (grey) patients. The blue segments inside or outside the bars indicate the median value of each fraction. The error bars indicate the standard error of the mean of each fraction. *p<0.05, **p<0.01, and ***p<0.001.

5. Discussion

Finding a significantly higher fraction of Tc1 and Th1 accompanied by an increased immune checkpoint expression in MSI colorectal cancer has also been suggested by other studies using non-immunohistochemistry-based methods. In agreement with our results, a study on 270 colorectal cancers using the TCGA dataset found higher gene expression of Th1 related signatures in MSI colorectal cancers compared to the MSS (7). In addition, another study on 598 colorectal cancers employing next-generation sequencing, also reported a higher gene expression of Th1 related signatures in MSI colorectal cancers (165). Furthermore, using qRT-PCR in a cohort of 25 colorectal cancers showed a higher genetic expression of type 1 cytotoxic and type 1 helper T-cell related genes in MSI-H compared to MSS colorectal cancers (188). Others utilizing single-cell RNA-seq analyses demonstrated a significantly increased T_H1-like cell signal in MSI patients in a cohort of 12 colorectal cancers (189). There is also rising evidence for increased TIM3 (190), CTLA-4 (188), and PD-1 (7) expression in MSI compared to MSS colorectal cancers. The concordance with our findings using a variety of methods can be seen as an indirect validation of our multiplex fluorescence BLEACH&STAIN analysis framework.

The increased fraction of Tc1 cytotoxic T-cells and Th1 helper T-cells accompanied by a strong interaction network between Tc1, Th1 and dendritic cells in MSI colorectal cancers compared to MSS patients, suggest a driving role in the enhanced anti-cancer immunity of a microsatellite instable tumor microenvironment. Thus, these findings correspond well to rising evidence that Th1 cells can acquire the ability to promote Tc1 cell survival, effector function, and tumor-adjacent localization by targeted delivery of cytokine IL-2 (13,191). Likewise, Tc1 cells were observed to promote the polarization of $CD4^+$ T cells towards a Th1 phenotype, enhancing the Tc1/Th1-mediated anticancer immune response (9). These findings fit well to the fact that distinct dendritic cell subpopulations can present tumor antigens to promote polarization of $CD8^+$ T-cells into type 1 cytotoxic T-cell (Tc1)(192,193). In agreement, recent evidence has demonstrated that vaccine-based rescue of dendritic cells can result in in vitro and in vivo cytotoxic T cell responses due to elevated Tc1 levels (194). Given that Tc1 cells are known as a cytotoxic T-cell subpopulation with superior cytotoxicity against tumor cells compared to other cytotoxic T-cell subsets (8-10), the “terminal end route” of anticancer immunity due to direct cell-to-cell contact-based tumor cell elimination might be represented by a high fraction of Tc1 cells that are in direct contact to enhancing Th1 and dendritic cells.

Finding a reduced fraction of Th17, Th2, regulatory T-cells along with the absence of a strong interaction network between these T-cells in MSI colorectal cancers but finding an enriched fraction and strong interaction network between Th17, Th2, Tregs, and dendritic cells in MSS

patients highlights a less conducive pro-tumorigenic microenvironment in MSI colorectal cancers and a pro-tumorigenic TME in MSS patients. Hence, there is evidence for a tumor promoting role of Th2 in colorectal cancers due to promoting epithelial to mesenchymal transition (16), tumor cell proliferation, invasion (195), and initiation as well as progression of colorectal cancer (196). In addition, some studies have shown that distinct dendritic cell subpopulations can promote Th2 differentiation and thus tumor progression (197,198) which fits very well with the strong interaction between DCs and Th2 exclusively found in MSS patients and its absence in the tumor microenvironment of MSI patients. However, the role of Th17 in colorectal cancer is controversial. Experimental models have demonstrated that Th17 cells contribute to intestinal tumorigenesis (18,19) and promote angiogenesis (20). In contrast, it has been also shown that Th17 can recruit highly cytotoxic $CD8^+$ T cells in the intraepithelial tumor compartment (21).

The identification of increased levels of immune checkpoint expression, particularly of TIM3, CLTA-4 and PD-1 in MSI colorectal cancers that are well known for a high pre-existing anti-tumor immunity underlines the concept that high levels of immune checkpoint expression do not hinder anti-cancer immunity in an inflamed tumor microenvironment. These findings are in line with data from our recent study in muscle-invasive urothelial carcinomas providing an example where a high expression of TIM3, PD-1, and CTLA-4 on immune cell subpopulations was linked to a favorable outcome in an inflamed immune phenotype (199). Others have also shown in several different entities that high levels of immune checkpoint expression do not necessarily imply a terminally exhausted immune environment (200). Thus, these findings underline the concept that a high degree of immune cell infiltration (i.e., a high degree of anticancer immunity) is accompanied by a physiologically necessary upregulation of immune checkpoint receptors to prevent an excessive unregulated “overinflammation” or eventually autoimmune reaction (201).

Finding the characteristic enrichment of Tc1 and Th1 in MSI patients compared to MSS patients in the center of the tumor but not at the invasive margin underlines the concept that the immune tumor microenvironment (iTME) in proximity to the cancer cells - thus in the center of the tumor – relies on different immune regulations compared to the ITME at the invasive margin. It is well known that the abundance of immune cells, particularly T-cells subpopulations is on average two to three times higher at the invasive margin compared to the center of the tumor (202,203). Accordingly, also immune suppressive T-cells subpopulations such as regulatory T cells and tumor associated macrophages were described enriched at the invasive margin compared to the center of the tumor (203,204). Furthermore, the accumulation of ($PD\text{-}L1^+$) myeloid cells and increased interactions with $PD\text{-}1^+$ T-cells at the invasive margin was found to contribute to the immune suppressing activity and drive tumor immune evasion (204,205). Moreover, the center of the tumor is known to have a hypoxic tumor microenvironment (TME), while the invasive margin is

known for an oxygen rich TME that regulates T-cell functionality (204). Therefore, the invasive margin and center of the tumor can be interpreted as two completely different compartments of the immune tumor microenvironment and the data from this study suggest assessment of T-cell subpopulations in the center of the tumor of colorectal cancers.

In conclusion, this study identified a higher fraction of type 1 cytotoxic T-cells (Tc1) and type 1 helper T-cells (Th1) with a strong and distinct spatial interplay accompanied by a paucity of Th17, Th2, and regulatory T-cells as a characteristic feature of MSI colorectal cancers, especially in comparison to MSS patients that showed an adverse spatial interaction profile.

6. Summary

Microsatellite instability (MSI) is a strong biomarker to predict response to immune checkpoint therapy and patient's outcome in colorectal cancer. Although enrichment of distinct T-cell subpopulations, such as type 1 cytotoxic T-cells (Tc1) or type 1 helper T-cells (Th1), have been identified to impact patient's outcome and response to immune checkpoint therapy, only little is known about the underlying changes in the composition of the immune tumor microenvironment.

To assess the density, composition, degree of functional marker expression, and spatial interplay of T-cell subpopulations in 79 MSI and 1045 microsatellite stable (MSS) colorectal cancers, a tissue microarray as well as large sections were stained with 19 antibodies directed against T-cell, antigen presenting cells, functional markers, and structural proteins using our BLEACH&STAIN multiplex fluorescence immunohistochemistry approach. A deep learning-based framework comprising > 20 different convolutional neuronal networks (U-Net and DeepLabv3$^+$) was developed for image analysis.

The composition of Type 1 (T-bet$^+$), Type 2 (GATA3$^+$), Type 17 (RORγT$^+$), NKT-like (CD56$^+$), regulatory (FOXP3$^+$), and follicular (BCL6$^+$) cytotoxic (CD3$^+$CD8$^+$) or helper (CD3$^+$CD4$^+$) T-cells showed marked differences between MSI and MSS patients. For instance, the fraction of Tc1 as well as Th1 was significantly higher ($p<0.001$ each) while the fraction of Tregs, Th2, Th17 T-cells was significantly lower ($p<0.05$) in MSI compared to MSS patients. The degree of TIM3, CTLA-4, and PD-1 expression on most T-cell subpopulations was significantly higher in MSI compared to MSS patients ($p<0.05$ each). Spatial analysis revealed increased interactions between Th1, Tc1, and dendritic cells in MSI patients while in MSS patients the strongest interactions were found between Tregs, Th17, Th2 and dendritic cells. The additional analysis of 12 large sections confirmed the observations from the TMA analysis in the center of the tumor and showed a divergent immune composition in the invasive margin.

Therefore, this study identified a higher fraction of Tc1 T-cells and Th1 T-cells accompanied by a paucity of regulatory T-cell, Th17 and Th2 T-cell subpopulations along with a distinct interaction profile as a hallmark of MSI compared to MSS colorectal cancers.

7. Zusammenfassung

Mikrosatelliteninstabilität (MSI) stellt einen starken prädiktiven Marker für das Ansprechen auf Immun-Checkpoint-Therapie und daher der Prognose von Patienten mit kolorektalem Karzinom dar. Auch wenn das erhöhte Auftreten von T-Lymphozyten Subpopulationen im immune Mikromilieu, wie zum Beispiel Typ 1 zytotoxische T-Zellen (Tc1) oder Typ 1 T-helfer-Zellen, zunehmend mit dem Gesamtüberleben und Ansprechen auf Immun-Checkpoint-Therapie in Verbindung gebracht werden konnte, ist nur wenig über die zugrundliegenden Veränderungen in der Komposition der T-Lymphozyten Subpopulationen im kolorektalen Karzinom bekannt.

Ziel der Studie war es die Dichte, Komposition, Expression von funktionellen Markern (z.B. Immune Checkpoints) und die topografische Beziehung zwischen verschiedenen T-Lymphozyten Subpopulationen in 79 MSI and 1045 mikrosatellitenstabilen (MSS) kolorektalen Karzinomen zu untersuchen. Hierfür wurden Tissue Microarrays (TMAs) und Großschnitte mit 19 verschiedenen Antikörpern mit unserer BELACH&STAIN multiplex Fluoreszenz Immunhistochemie Methode zur Identifikation von mehr als 30 verschiedenen (funktionellen) T-Zell Subpopulationen sowie professionell Antigen präsentierenden Zellen gefärbt. Ein auf künstlicher Intelligenz (Deep Learning) basierter Algorithmus bestehend aus > 20 verschiedenen einzelnen neuronalen Netzen (U-Net und DeepLabv3$^+$) wurde für die Bildanalyse entwickelt und verwendet.

Die Komposition (Prozentuales Verhältnis der einzelnen T-Zell Subpopulationen an allen T-Zellen) von Typ 1 (T-bet$^+$), Typ 2 (GATA3$^+$), Typ 17 (RORγT$^+$), NKT-ähnlich (CD56$^+$), regulatorischen (FOXP3$^+$) und follikulären (BCL6$^+$) zytotoxischen (CD3$^+$CD8$^+$) oder Helfer (CD3$^+$CD4$^+$) T-Zellen zeigte signifikante Unterscheide zwischen MSI und MSS Patienten mit kolorektalen Karzinomen. Zum Beispiel war der Anteil an Tc1 und Th1 signifikant höher (jeweils $p<0,001$), während der Anteil von Tregs, Th2, Th17 T-Zellen signifikant geringer (jeweils $p<0,05$) in MSI im Vergleich zu MSS Patienten war. Der Grad der TIM3, CTLA-4 und PD-1 Expression auf den meisten T-Zell subpopulationen war signifikant höher in MSI im Vergleich zu MSS Patienten (jeweils $p<0,05$). Die Analyse der topografischen Beziehungen zeigte ein erhöhtes Interaktionsprofil zwischen Th1, Tc1 und dendritischen Zellen in MSI Patienten, während in MSS Pateinten ein erhöhtes Interaktionsprofil zwischen Tregs, Th17, Th2 und dendritisch Zellen gefunden wurde. Die ergänzende Analyse von 12 Großschnitten bestätigte die Ergebnisse aus der TMA Analyse aus dem Tumorzentrum und zeigte zusätzlich eine divergente Komposition der T-Zellen an der Invasionsfront auf.

Die Daten dieser Studie konnten einen höheren Anteil von Tc1 und Th1 T-Lymphozyten, einen geringen Anteil von FOXP3$^+$ regulatorischen, Th17 und Th2 T-Zell Subpopulationen, sowie ein spezifisches Interaktionsprofil als Charakteristikum des immun Tumormikromilieus von MSI kolorektalen Karzinomen aufzeigen.

8. References

1. Aaltonen LA, Salovaara R, Kristo P, Canzian F, Hemminki A, Peltomäki P*, et al.* Incidence of hereditary nonpolyposis colorectal cancer and the feasibility of molecular screening for the disease. N Engl J Med **1998**;338:1481-7
2. Hampel H, Frankel WL, Martin E, Arnold M, Khanduja K, Kuebler P*, et al.* Screening for the Lynch syndrome (hereditary nonpolyposis colorectal cancer). N Engl J Med **2005**;352:1851-60
3. Sinicrope FA, Rego RL, Halling KC, Foster N, Sargent DJ, La Plant B*, et al.* Prognostic impact of microsatellite instability and DNA ploidy in human colon carcinoma patients. Gastroenterology **2006**;131:729-37
4. Cercek A, Lumish M, Sinopoli J, Weiss J, Shia J, Lamendola-Essel M*, et al.* PD-1 Blockade in Mismatch Repair-Deficient, Locally Advanced Rectal Cancer. N Engl J Med **2022**;386:2363-76
5. Goodman AM, Sokol ES, Frampton GM, Lippman SM, Kurzrock R. Microsatellite-Stable Tumors with High Mutational Burden Benefit from Immunotherapy. Cancer Immunol Res **2019**;7:1570-3
6. Ionov Y, Peinado MA, Malkhosyan S, Shibata D, Perucho M. Ubiquitous somatic mutations in simple repeated sequences reveal a new mechanism for colonic carcinogenesis. Nature **1993**;363:558-61
7. Mlecnik B, Bindea G, Angell HK, Maby P, Angelova M, Tougeron D*, et al.* Integrative Analyses of Colorectal Cancer Show Immunoscore Is a Stronger Predictor of Patient Survival Than Microsatellite Instability. Immunity **2016**;44:698-711
8. St Paul M, Ohashi PS. The Roles of CD8(+) T Cell Subsets in Antitumor Immunity. Trends Cell Biol **2020**;30:695-704
9. Ye Z, Tang C, Xu S, Zhang B, Zhang X, Moyana T*, et al.* Type 1 CD8+ T cells are superior to type 2 CD8+ T cells in tumor immunotherapy due to their efficient cytotoxicity, prolonged survival and type 1 immune modulation. Cell Mol Immunol **2007**;4:277-85
10. Nishimura F, Dusak JE, Eguchi J, Zhu X, Gambotto A, Storkus WJ*, et al.* Adoptive transfer of type 1 CTL mediates effective anti-central nervous system tumor response: critical roles of IFN-inducible protein-10. Cancer Res **2006**;66:4478-87
11. Kemp RA, Ronchese F. Tumor-specific Tc1, but not Tc2, cells deliver protective antitumor immunity. J Immunol **2001**;167:6497-502
12. Chaput N, Louafi S, Bardier A, Charlotte F, Vaillant JC, Menegaux F*, et al.* Identification of CD8+CD25+Foxp3+ suppressive T cells in colorectal cancer tissue. Gut **2009**;58:520-9
13. Huang H, Hao S, Li F, Ye Z, Yang J, Xiang J. CD4+ Th1 cells promote CD8+ Tc1 cell survival, memory response, tumor localization and therapy by targeted delivery of interleukin 2 via acquired pMHC I complexes. Immunology **2007**;120:148-59
14. Kim HJ, Cantor H. CD4 T-cell subsets and tumor immunity: the helpful and the not-so-helpful. Cancer Immunol Res **2014**;2:91-8
15. Nishimura T, Iwakabe K, Sekimoto M, Ohmi Y, Yahata T, Nakui M*, et al.* Distinct role of antigen-specific T helper type 1 (Th1) and Th2 cells in tumor eradication in vivo. J Exp Med **1999**;190:617-27
16. Chen J, Gong C, Mao H, Li Z, Fang Z, Chen Q*, et al.* E2F1/SP3/STAT6 axis is required for IL-4-induced epithelial-mesenchymal transition of colorectal cancer cells. Int J Oncol **2018**;53:567-78
17. Mattes J, Hulett M, Xie W, Hogan S, Rothenberg ME, Foster P*, et al.* Immunotherapy of cytotoxic T cell-resistant tumors by T helper 2 cells: an eotaxin and STAT6-dependent process. J Exp Med **2003**;197:387-93
18. Wang K, Kim MK, Di Caro G, Wong J, Shalapour S, Wan J*, et al.* Interleukin-17 receptor a signaling in transformed enterocytes promotes early colorectal tumorigenesis. Immunity **2014**;41:1052-63
19. Grivennikov SI, Wang K, Mucida D, Stewart CA, Schnabl B, Jauch D*, et al.* Adenoma-linked barrier defects and microbial products drive IL-23/IL-17-mediated tumour growth. Nature **2012**;491:254-8

20. Chung AS, Wu X, Zhuang G, Ngu H, Kasman I, Zhang J*, et al.* An interleukin-17-mediated paracrine network promotes tumor resistance to anti-angiogenic therapy. Nat Med **2013**;19:1114-23
21. Amicarella F, Muraro MG, Hirt C, Cremonesi E, Padovan E, Mele V*, et al.* Dual role of tumour-infiltrating T helper 17 cells in human colorectal cancer. Gut **2017**;66:692-704
22. Whiteside TL. What are regulatory T cells (Treg) regulating in cancer and why? Semin Cancer Biol **2012**;22:327-34
23. Sung H, Ferlay J, Siegel RL, Laversanne M, Soerjomataram I, Jemal A*, et al.* Global Cancer Statistics 2020: GLOBOCAN Estimates of Incidence and Mortality Worldwide for 36 Cancers in 185 Countries. CA Cancer J Clin **2021**;71:209-49
24. Triantafillidis JK, Nasioulas G, Kosmidis PA. Colorectal cancer and inflammatory bowel disease: epidemiology, risk factors, mechanisms of carcinogenesis and prevention strategies. Anticancer Res **2009**;29:2727-37
25. Edwards BK, Ward E, Kohler BA, Eheman C, Zauber AG, Anderson RN*, et al.* Annual report to the nation on the status of cancer, 1975-2006, featuring colorectal cancer trends and impact of interventions (risk factors, screening, and treatment) to reduce future rates. Cancer **2010**;116:544-73
26. Fleming M, Ravula S, Tatishchev SF, Wang HL. Colorectal carcinoma: Pathologic aspects. J Gastrointest Oncol **2012**;3:153-73
27. Nagtegaal ID, Odze RD, Klimstra D, Paradis V, Rugge M, Schirmacher P*, et al.* The 2019 WHO classification of tumours of the digestive system. Histopathology **2020**;76:182-8
28. Petrelli F, Tomasello G, Borgonovo K, Ghidini M, Turati L, Dallera P*, et al.* Prognostic Survival Associated With Left-Sided vs Right-Sided Colon Cancer: A Systematic Review and Meta-analysis. JAMA Oncol **2017**;3:211-9
29. Nojadeh JN, Behrouz Sharif S, Sakhinia E. Microsatellite instability in colorectal cancer. Excli j **2018**;17:159-68
30. Guinney J, Dienstmann R, Wang X, de Reyniès A, Schlicker A, Soneson C*, et al.* The consensus molecular subtypes of colorectal cancer. Nat Med **2015**;21:1350-6
31. Ten Hoorn S, de Back TR, Sommeijer DW, Vermeulen L. Clinical Value of Consensus Molecular Subtypes in Colorectal Cancer: A Systematic Review and Meta-Analysis. J Natl Cancer Inst **2022**;114:503-16
32. Navarro M, Nicolas A, Ferrandez A, Lanas A. Colorectal cancer population screening programs worldwide in 2016: An update. World J Gastroenterol **2017**;23:3632-42
33. Winawer SJ, Fletcher RH, Miller L, Godlee F, Stolar MH, Mulrow CD*, et al.* Colorectal cancer screening: clinical guidelines and rationale. Gastroenterology **1997**;112:594-642
34. Winawer SJ, Zauber AG, Ho MN, O'Brien MJ, Gottlieb LS, Sternberg SS*, et al.* Prevention of colorectal cancer by colonoscopic polypectomy. The National Polyp Study Workgroup. N Engl J Med **1993**;329:1977-81
35. Ciccolallo L, Capocaccia R, Coleman MP, Berrino F, Coebergh JW, Damhuis RA*, et al.* Survival differences between European and US patients with colorectal cancer: role of stage at diagnosis and surgery. Gut **2005**;54:268-73
36. Garcia-Etxebarria K, Clos-Garcia M, Telleria O, Nafría B, Alonso C, Iruarrizaga-Lejarreta M*, et al.* Interplay between Genome, Metabolome and Microbiome in Colorectal Cancer. Cancers (Basel) **2021**;13
37. Keum N, Giovannucci E. Global burden of colorectal cancer: emerging trends, risk factors and prevention strategies. Nat Rev Gastroenterol Hepatol **2019**;16:713-32
38. Boland CR, Goel A. Microsatellite instability in colorectal cancer. Gastroenterology **2010**;138:2073-87.e3
39. Pećina-Šlaus N, Kafka A, Salamon I, Bukovac A. Mismatch Repair Pathway, Genome Stability and Cancer. Front Mol Biosci **2020**;7:122
40. Arulananda S, Thapa B, Walkiewicz M, Zapparoli GV, Williams DS, Dobrovic A*, et al.* Mismatch Repair Protein Defects and Microsatellite Instability in Malignant Pleural Mesothelioma. J Thorac Oncol **2018**;13:1588-94

41. Cheah PL, Li J, Looi LM, Koh CC, Lau TP, Chang SW*, et al.* Screening for microsatellite instability in colorectal carcinoma: Practical utility of immunohistochemistry and PCR with fragment analysis in a diagnostic histopathology setting. Malays J Pathol **2019**;41:91-100
42. Boland CR, Thibodeau SN, Hamilton SR, Sidransky D, Eshleman JR, Burt RW*, et al.* A National Cancer Institute Workshop on Microsatellite Instability for cancer detection and familial predisposition: development of international criteria for the determination of microsatellite instability in colorectal cancer. Cancer Res **1998**;58:5248-57
43. Bacher JW, Flanagan LA, Smalley RL, Nassif NA, Burgart LJ, Halberg RB*, et al.* Development of a fluorescent multiplex assay for detection of MSI-High tumors. Dis Markers **2004**;20:237-50
44. Berardinelli GN, Scapulatempo-Neto C, Durães R, Antônio de Oliveira M, Guimarães D, Reis RM. Advantage of HSP110 (T17) marker inclusion for microsatellite instability (MSI) detection in colorectal cancer patients. Oncotarget **2018**;9:28691-701
45. Wang DY, Salem JE, Cohen JV, Chandra S, Menzer C, Ye F*, et al.* Fatal Toxic Effects Associated With Immune Checkpoint Inhibitors: A Systematic Review and Meta-analysis. JAMA Oncol **2018**;4:1721-8
46. Hempelmann JA, Lockwood CM, Konnick EQ, Schweizer MT, Antonarakis ES, Lotan TL*, et al.* Microsatellite instability in prostate cancer by PCR or next-generation sequencing. J Immunother Cancer **2018**;6:29
47. Cheng DT, Prasad M, Chekaluk Y, Benayed R, Sadowska J, Zehir A*, et al.* Comprehensive detection of germline variants by MSK-IMPACT, a clinical diagnostic platform for solid tumor molecular oncology and concurrent cancer predisposition testing. BMC Med Genomics **2017**;10:33
48. First Comprehensive Companion Diagnostic OK'd. Cancer Discov **2018**;8:Of4
49. Buckowitz A, Knaebel HP, Benner A, Bläker H, Gebert J, Kienle P*, et al.* Microsatellite instability in colorectal cancer is associated with local lymphocyte infiltration and low frequency of distant metastases. Br J Cancer **2005**;92:1746-53
50. Berg KD, Glaser CL, Thompson RE, Hamilton SR, Griffin CA, Eshleman JR. Detection of microsatellite instability by fluorescence multiplex polymerase chain reaction. J Mol Diagn **2000**;2:20-8
51. Popat S, Hubner R, Houlston RS. Systematic review of microsatellite instability and colorectal cancer prognosis. J Clin Oncol **2005**;23:609-18
52. Petrelli F, Ghidini M, Cabiddu M, Pezzica E, Corti D, Turati L*, et al.* Microsatellite Instability and Survival in Stage II Colorectal Cancer: A Systematic Review and Meta-analysis. Anticancer Res **2019**;39:6431-41
53. Quintanilha JCF, Graf RP, Fisher VA, Oxnard GR, Ellis H, Panarelli N*, et al.* Comparative Effectiveness of Immune Checkpoint Inhibitors vs Chemotherapy in Patients With Metastatic Colorectal Cancer With Measures of Microsatellite Instability, Mismatch Repair, or Tumor Mutational Burden. JAMA Netw Open **2023**;6:e2252244
54. Le DT, Uram JN, Wang H, Bartlett BR, Kemberling H, Eyring AD*, et al.* PD-1 Blockade in Tumors with Mismatch-Repair Deficiency. N Engl J Med **2015**;372:2509-20
55. Le DT, Durham JN, Smith KN, Wang H, Bartlett BR, Aulakh LK*, et al.* Mismatch repair deficiency predicts response of solid tumors to PD-1 blockade. Science **2017**;357:409-13
56. Mlecnik B, Bindea G, Angell HK, Maby P, Angelova M, Tougeron D*, et al.* Integrative Analyses of Colorectal Cancer Show Immunoscore Is a Stronger Predictor of Patient Survival Than Microsatellite Instability. Immunity **2016**;44:698-711
57. Lu L, Liu YJ, Cheng PQ, Hu D, Xu HC, Ji G. Macrophages play a role in inflammatory transformation of colorectal cancer. World J Gastrointest Oncol **2021**;13:2013-28
58. Huang F, Wang Y, Shao Y, Zhang R, Li M, Liu L*, et al.* M2 Macrophage Classification of Colorectal Cancer Reveals Intrinsic Connections with Metabolism Reprogramming and Clinical Characteristics. Pharmgenomics Pers Med **2024**;17:383-99
59. Yang C, Wei C, Wang S, Shi D, Zhang C, Lin X*, et al.* Elevated CD163(+)/CD68(+) Ratio at Tumor Invasive Front is Closely Associated with Aggressive Phenotype and Poor Prognosis in Colorectal Cancer. Int J Biol Sci **2019**;15:984-98

60. Konstantinov AS, Kovaleva OV, Samoilova DV, Shelekhova KV. Role of macrophages in progression of colorectal cancer: a contrast with the traditional paradigm. Int J Clin Exp Pathol **2022**;15:403-11
61. Zhou Q, Peng RQ, Wu XJ, Xia Q, Hou JH, Ding Y*, et al.* The density of macrophages in the invasive front is inversely correlated to liver metastasis in colon cancer. J Transl Med **2010**;8:13
62. Wang H, Tian T, Zhang J. Tumor-Associated Macrophages (TAMs) in Colorectal Cancer (CRC): From Mechanism to Therapy and Prognosis. Int J Mol Sci **2021**;22
63. Lee YS, Song SJ, Hong HK, Oh BY, Lee WY, Cho YB. The FBW7-MCL-1 axis is key in M1 and M2 macrophage-related colon cancer cell progression: validating the immunotherapeutic value of targeting PI3Kγ. Exp Mol Med **2020**;52:815-31
64. Li Y, Chen Z, Han J, Ma X, Zheng X, Chen J. Functional and Therapeutic Significance of Tumor-Associated Macrophages in Colorectal Cancer. Front Oncol **2022**;12:781233
65. Wei C, Yang C, Wang S, Shi D, Zhang C, Lin X*, et al.* Crosstalk between cancer cells and tumor associated macrophages is required for mesenchymal circulating tumor cell-mediated colorectal cancer metastasis. Mol Cancer **2019**;18:64
66. Yuan M, Zhang X, Zhang J, Wang K, Zhang Y, Shang W*, et al.* DC-SIGN-LEF1/TCF1-miR-185 feedback loop promotes colorectal cancer invasion and metastasis. Cell Death Differ **2020**;27:379-95
67. Gessani S, Belardelli F. Immune Dysfunctions and Immunotherapy in Colorectal Cancer: The Role of Dendritic Cells. Cancers (Basel) **2019**;11
68. Wooster AL, Girgis LH, Brazeale H, Anderson TS, Wood LM, Lowe DB. Dendritic cell vaccine therapy for colorectal cancer. Pharmacol Res **2021**;164:105374
69. Perez CR, De Palma M. Engineering dendritic cell vaccines to improve cancer immunotherapy. Nat Commun **2019**;10:5408
70. Subtil B, Cambi A, Tauriello DVF, de Vries IJM. The Therapeutic Potential of Tackling Tumor-Induced Dendritic Cell Dysfunction in Colorectal Cancer. Front Immunol **2021**;12:724883
71. Yin K, Xia X, Rui K, Wang T, Wang S. Myeloid-Derived Suppressor Cells: A New and Pivotal Player in Colorectal Cancer Progression. Front Oncol **2020**;10:610104
72. Shi H, Li K, Ni Y, Liang X, Zhao X. Myeloid-Derived Suppressor Cells: Implications in the Resistance of Malignant Tumors to T Cell-Based Immunotherapy. Front Cell Dev Biol **2021**;9:707198
73. Song F, Zhang Y, Chen Q, Bi D, Yang M, Lu L*, et al.* Mast cells inhibit colorectal cancer development by inducing ER stress through secreting Cystatin C. Oncogene **2023**;42:209-23
74. Liu X, Li X, Wei H, Liu Y, Li N. Mast cells in colorectal cancer tumour progression, angiogenesis, and lymphangiogenesis. Front Immunol **2023**;14:1209056
75. Deng L, Jiang N, Zeng J, Wang Y, Cui H. The Versatile Roles of Cancer-Associated Fibroblasts in Colorectal Cancer and Therapeutic Implications. Front Cell Dev Biol **2021**;9:733270
76. Zhong B, Cheng B, Huang X, Xiao Q, Niu Z, Chen YF*, et al.* Colorectal cancer-associated fibroblasts promote metastasis by up-regulating LRG1 through stromal IL-6/STAT3 signaling. Cell Death Dis **2021**;13:16
77. Liu T, Han C, Wang S, Fang P, Ma Z, Xu L*, et al.* Cancer-associated fibroblasts: an emerging target of anti-cancer immunotherapy. J Hematol Oncol **2019**;12:86
78. Wang Y, Zhong X, He X, Hu Z, Huang H, Chen J*, et al.* Liver metastasis from colorectal cancer: pathogenetic development, immune landscape of the tumour microenvironment and therapeutic approaches. J Exp Clin Cancer Res **2023**;42:177
79. Montauti E, Oh DY, Fong L. CD4(+) T cells in antitumor immunity. Trends Cancer **2024**;10:969-85
80. Wang J, Lou Y, Wang S, Zhang Z, You J, Zhu Y*, et al.* IFNγ at the early stage induced after cryo-thermal therapy maintains CD4(+) Th1-prone differentiation, leading to long-term antitumor immunity. Front Immunol **2024**;15:1345046
81. Karachaliou N, Gonzalez-Cao M, Crespo G, Drozdowskyj A, Aldeguer E, Gimenez-Capitan A*, et al.* Interferon gamma, an important marker of response to immune checkpoint blockade in non-small cell lung cancer and melanoma patients. Ther Adv Med Oncol **2018**;10:1758834017749748

82. Cao Q, Xue R, Zhang N. Th1 cells inducing IFNγ response improves immunotherapy efficacy in gastric cancer. Chin J Cancer Res **2023**;35:299-315
83. Franken A, Bila M, Mechels A, Kint S, Van Dessel J, Pomella V*, et al.* CD4(+) T cell activation distinguishes response to anti-PD-L1+anti-CTLA4 therapy from anti-PD-L1 monotherapy. Immunity **2024**;57:541-58.e7
84. Schreiber S, Hammers CM, Kaasch AJ, Schraven B, Dudeck A, Kahlfuss S. Metabolic Interdependency of Th2 Cell-Mediated Type 2 Immunity and the Tumor Microenvironment. Front Immunol **2021**;12:632581
85. Andreu-Sanz D, Kobold S. Role and Potential of Different T Helper Cell Subsets in Adoptive Cell Therapy. Cancers (Basel) **2023**;15
86. Jacenik D, Karagiannidis I, Beswick EJ. Th2 cells inhibit growth of colon and pancreas cancers by promoting anti-tumorigenic responses from macrophages and eosinophils. Br J Cancer **2023**;128:387-97
87. Lorvik KB, Hammarström C, Fauskanger M, Haabeth OA, Zangani M, Haraldsen G*, et al.* Adoptive Transfer of Tumor-Specific Th2 Cells Eradicates Tumors by Triggering an In Situ Inflammatory Immune Response. Cancer Res **2016**;76:6864-76
88. Foerster F, Hess M, Gerhold-Ay A, Marquardt JU, Becker D, Galle PR*, et al.* The immune contexture of hepatocellular carcinoma predicts clinical outcome. Sci Rep **2018**;8:5351
89. Wang T, Tang L, Ouyang B, Chen X, Qi J. Clinical significance and changes to the immune microenvironment of colorectal cancer patients with liver metastasis. J Gastrointest Oncol **2023**;14:206-12
90. Lin CM, Lin LW, Chen YW, Ye YL. The expression and prognostic impact of proinflammatory cytokines and their associations with carcinogens in oropharyngeal squamous cell carcinoma. Cancer Immunol Immunother **2020**;69:549-58
91. Cao Z, Jing Y, Cheng C, Wang F, Guan M, Zhang K*, et al.* EIF2Ss, a Novel c-Myc-Correlated Gene Family, is Associated with Poor Prognosis and Immune Infiltration in Pancreatic Adenocarcinoma. Front Biosci (Landmark Ed) **2024**;29:119
92. Bettelli E, Carrier Y, Gao W, Korn T, Strom TB, Oukka M*, et al.* Reciprocal developmental pathways for the generation of pathogenic effector TH17 and regulatory T cells. Nature **2006**;441:235-8
93. Qianmei Y, Zehong S, Guang W, Hui L, Lian G. Recent advances in the role of Th17/Treg cells in tumor immunity and tumor therapy. Immunol Res **2021**;69:398-414
94. Ma M, Huang W, Kong D. IL-17 inhibits the accumulation of myeloid-derived suppressor cells in breast cancer via activating STAT3. Int Immunopharmacol **2018**;59:148-56
95. Ye J, Livergood RS, Peng G. The role and regulation of human Th17 cells in tumor immunity. Am J Pathol **2013**;182:10-20
96. Ma K, Yang L, Shen R, Kong B, Chen W, Liang J*, et al.* Th17 cells regulate the production of CXCL1 in breast cancer. Int Immunopharmacol **2018**;56:320-9
97. Hamaï A, Pignon P, Raimbaud I, Duperrier-Amouriaux K, Senellart H, Hiret S*, et al.* Human T(H)17 immune cells specific for the tumor antigen MAGE-A3 convert to IFN-γ-secreting cells as they differentiate into effector T cells in vivo. Cancer Res **2012**;72:1059-63
98. Rocha Martins P, Luciano Pereira Morais K, de Lima Galdino NA, Jacauna A, Paula SOC, Magalhães WCS*, et al.* Linking tumor immune infiltrate and systemic immune mediators to treatment response and prognosis in advanced cervical cancer. Sci Rep **2023**;13:22634
99. Zhao RD, Liu DJ, Li JW, Wang Y, Lin JH, Zhang YT*, et al.* Landscape and prognostic values of lymphocytes in patients with hepatocellular carcinoma undergoing transarterial embolization. J Leukoc Biol **2024**;116:186-96
100. Dai S, Liu T, Liu XQ, Li XY, Xu K, Ren T*, et al.* Identification of an Immune-Related Signature Predicting Survival Risk and Immune Microenvironment in Gastric Cancer. Front Cell Dev Biol **2021**;9:687473
101. Avalos-Navarro G, Muñoz-Valle JF, Daneri-Navarro A, Quintero-Ramos A, Franco-Topete RA, Morán-Mendoza AJ*, et al.* Circulating soluble levels of MIF in women with breast cancer in the molecular subtypes: relationship with Th17 cytokine profile. Clin Exp Med **2019**;19:385-91

102. Theobald L, Stroeder R, Melchior P, Iordache, II, Tänzer T, Port M*, et al.* Chemoradiotherapy-induced increase in Th17 cell frequency in cervical cancer patients is associated with therapy resistance and early relapse. Mol Oncol **2021**;15:3559-77
103. Ding H, Xu JC, Ding ZG, Wu LF, Liu YB, Zhang YF*, et al.* Identification and validation of UBE2B as a prognostic biomarker promoting the development of esophageal carcinomas. Front Immunol **2024**;15:1295305
104. Schmälter AK, Löhr P, Konrad M, Waidhauser J, Arndt TT, Schiele S*, et al.* Alterations in Peripheral Lymphocyte Subsets under Immunochemotherapy in Stage IV SCLC Patients: Th17 Cells as Potential Early Predictive Biomarker for Response. Int J Mol Sci **2024**;25
105. Sha H, Tong F, Ni J, Sun Y, Zhu Y, Qi L*, et al.* First-line penpulimab (an anti-PD1 antibody) and anlotinib (an angiogenesis inhibitor) with nab-paclitaxel/gemcitabine (PAAG) in metastatic pancreatic cancer: a prospective, multicentre, biomolecular exploratory, phase II trial. Signal Transduct Target Ther **2024**;9:143
106. Gutiérrez-Melo N, Baumjohann D. T follicular helper cells in cancer. Trends Cancer **2023**;9:309-25
107. Wang J, Jiang D, Zheng X, Li W, Zhao T, Wang D*, et al.* Tertiary lymphoid structure and decreased CD8(+) T cell infiltration in minimally invasive adenocarcinoma. iScience **2022**;25:103883
108. Garaud S, Buisseret L, Solinas C, Gu-Trantien C, de Wind A, Van den Eynden G*, et al.* Tumor infiltrating B-cells signal functional humoral immune responses in breast cancer. JCI Insight **2019**;5
109. Goubet AG, Lordello L, Alves Costa Silva C, Peguillet I, Gazzano M, Mbogning-Fonkou MD*, et al.* Escherichia coli-Specific CXCL13-Producing TFH Are Associated with Clinical Efficacy of Neoadjuvant PD-1 Blockade against Muscle-Invasive Bladder Cancer. Cancer Discov **2022**;12:2280-307
110. Quezada SA, Peggs KS, Curran MA, Allison JP. CTLA4 blockade and GM-CSF combination immunotherapy alters the intratumor balance of effector and regulatory T cells. J Clin Invest **2006**;116:1935-45
111. Paluskievicz CM, Cao X, Abdi R, Zheng P, Liu Y, Bromberg JS. T Regulatory Cells and Priming the Suppressive Tumor Microenvironment. Front Immunol **2019**;10:2453
112. Montauti E, Weinberg SE, Chu P, Chaudhuri S, Mani NL, Iyer R*, et al.* A deubiquitination module essential for T(reg) fitness in the tumor microenvironment. Sci Adv **2022**;8:eabo4116
113. Tay C, Tanaka A, Sakaguchi S. Tumor-infiltrating regulatory T cells as targets of cancer immunotherapy. Cancer Cell **2023**;41:450-65
114. Peng GL, Li L, Guo YW, Yu P, Yin XJ, Wang S*, et al.* CD8(+) cytotoxic and FoxP3(+) regulatory T lymphocytes serve as prognostic factors in breast cancer. Am J Transl Res **2019**;11:5039-53
115. Hayashi Y, Ueyama A, Funaki S, Jinushi K, Higuchi N, Morihara H*, et al.* In situ analysis of CCR8(+) regulatory T cells in lung cancer: suppression of GzmB(+) CD8(+) T cells and prognostic marker implications. BMC Cancer **2024**;24:627
116. Liu Y, Shan F, Sun Y, Kai H, Cao Y, Huang M*, et al.* Prognostic and immunotherapeutic potential of regulatory T cell-associated signature in ovarian cancer. J Cell Mol Med **2024**;28:e18248
117. Ito N, Suzuki Y, Taniguchi Y, Ishiguro K, Nakamura H, Ohgi S. Prognostic significance of T helper 1 and 2 and T cytotoxic 1 and 2 cells in patients with non-small cell lung cancer. Anticancer Res **2005**;25:2027-31
118. Faghih Z, Rezaeifard S, Safaei A, Ghaderi A, Erfani N. IL-17 and IL-4 producing CD8+ T cells in tumor draining lymph nodes of breast cancer patients: positive association with tumor progression. Iran J Immunol **2013**;10:193-204
119. Podhorecka M, Dmoszynska A, Rolinski J, Wasik E. T type 1/type 2 subsets balance in B-cell chronic lymphocytic leukemia--the three-color flow cytometry analysis. Leuk Res **2002**;26:657-60
120. Sun Y, Zhai C, Chen X, Dong Z, Hou L, Zhou C*, et al.* Characterization of PD-L1 protein expression and CD8(+) tumor-infiltrating lymphocyte density, and their associations with clinical outcome in small-cell lung cancer. Transl Lung Cancer Res **2019**;8:748-59

121. Brambilla E, Le Teuff G, Marguet S, Lantuejoul S, Dunant A, Graziano S*, et al.* Prognostic Effect of Tumor Lymphocytic Infiltration in Resectable Non-Small-Cell Lung Cancer. J Clin Oncol **2016**;34:1223-30
122. Maleki Vareki S. High and low mutational burden tumors versus immunologically hot and cold tumors and response to immune checkpoint inhibitors. J Immunother Cancer **2018**;6:157
123. Zhang J, Huang D, Saw PE, Song E. Turning cold tumors hot: from molecular mechanisms to clinical applications. Trends Immunol **2022**;43:523-45
124. Nicolet BP, Guislain A, van Alphen FPJ, Gomez-Eerland R, Schumacher TNM, van den Biggelaar M*, et al.* CD29 identifies IFN-γ-producing human CD8(+) T cells with an increased cytotoxic potential. Proc Natl Acad Sci U S A **2020**;117:6686-96
125. Coyle AJ, Erard F, Bertrand C, Walti S, Pircher H, Le Gros G. Virus-specific CD8+ cells can switch to interleukin 5 production and induce airway eosinophilia. J Exp Med **1995**;181:1229-33
126. Sad S, Marcotte R, Mosmann TR. Cytokine-induced differentiation of precursor mouse CD8+ T cells into cytotoxic CD8+ T cells secreting Th1 or Th2 cytokines. Immunity **1995**;2:271-9
127. Croft M, Carter L, Swain SL, Dutton RW. Generation of polarized antigen-specific CD8 effector populations: reciprocal action of interleukin (IL)-4 and IL-12 in promoting type 2 versus type 1 cytokine profiles. J Exp Med **1994**;180:1715-28
128. Hinks TSC, Hoyle RD, Gelfand EW. CD8(+) Tc2 cells: underappreciated contributors to severe asthma. Eur Respir Rev **2019**;28
129. Hilvering B, Hinks TSC, Stöger L, Marchi E, Salimi M, Shrimanker R*, et al.* Synergistic activation of pro-inflammatory type-2 CD8(+) T lymphocytes by lipid mediators in severe eosinophilic asthma. Mucosal Immunol **2018**;11:1408-19
130. Do JS, Choi YH, Shin SH, Yi HK, Hwang PH, Nam SY. Committed memory effector type 2 cytotoxic T (Tc2) cells are ineffective in protective anti-tumor immunity. Immunol Lett **2004**;95:77-84
131. Sheu BC, Lin RH, Lien HC, Ho HN, Hsu SM, Huang SC. Predominant Th2/Tc2 polarity of tumor-infiltrating lymphocytes in human cervical cancer. J Immunol **2001**;167:2972-8
132. Hartana CA, Ahlén Bergman E, Zirakzadeh AA, Krantz D, Winerdal ME, Winerdal M*, et al.* Urothelial bladder cancer may suppress perforin expression in CD8+ T cells by an ICAM-1/TGFβ2 mediated pathway. PLoS One **2018**;13:e0200079
133. Lückel C, Picard FSR, Huber M. Tc17 biology and function: Novel concepts. Eur J Immunol **2020**;50:1257-67
134. Chellappa S, Hugenschmidt H, Hagness M, Subramani S, Melum E, Line PD*, et al.* CD8+ T Cells That Coexpress RORγt and T-bet Are Functionally Impaired and Expand in Patients with Distal Bile Duct Cancer. J Immunol **2017**;198:1729-39
135. Hamada H, Garcia-Hernandez Mde L, Reome JB, Misra SK, Strutt TM, McKinstry KK*, et al.* Tc17, a unique subset of CD8 T cells that can protect against lethal influenza challenge. J Immunol **2009**;182:3469-81
136. Res PC, Piskin G, de Boer OJ, van der Loos CM, Teeling P, Bos JD*, et al.* Overrepresentation of IL-17A and IL-22 producing CD8 T cells in lesional skin suggests their involvement in the pathogenesis of psoriasis. PLoS One **2010**;5:e14108
137. Harrison OJ, Linehan JL, Shih HY, Bouladoux N, Han SJ, Smelkinson M*, et al.* Commensal-specific T cell plasticity promotes rapid tissue adaptation to injury. Science **2019**;363
138. Flores-Santibáñez F, Cuadra B, Fernández D, Rosemblatt MV, Núñez S, Cruz P*, et al.* In Vitro-Generated Tc17 Cells Present a Memory Phenotype and Serve As a Reservoir of Tc1 Cells In Vivo. Front Immunol **2018**;9:209
139. Kim BS, Kuen DS, Koh CH, Kim HD, Chang SH, Kim S*, et al.* Type 17 immunity promotes the exhaustion of CD8(+) T cells in cancer. J Immunother Cancer **2021**;9
140. Kong X, Sun R, Chen Y, Wei H, Tian Z. γδT cells drive myeloid-derived suppressor cell-mediated CD8+ T cell exhaustion in hepatitis B virus-induced immunotolerance. J Immunol **2014**;193:1645-53
141. Tao J, Han D, Gao S, Zhang W, Yu H, Liu P*, et al.* CD8(+) T cells exhaustion induced by myeloid-derived suppressor cells in myelodysplastic syndromes patients might be through TIM3/Gal-9 pathway. J Cell Mol Med **2020**;24:1046-58

142. Mishra S, Srinivasan S, Ma C, Zhang N. CD8(+) Regulatory T Cell - A Mystery to Be Revealed. Front Immunol **2021**;12:708874
143. Jiang H, Zhang SI, Pernis B. Role of CD8+ T cells in murine experimental allergic encephalomyelitis. Science **1992**;256:1213-5
144. Koh DR, Fung-Leung WP, Ho A, Gray D, Acha-Orbea H, Mak TW. Less mortality but more relapses in experimental allergic encephalomyelitis in CD8-/- mice. Science **1992**;256:1210-3
145. Romero-Olmedo AJ, Schulz AR, Huber M, Brehm CU, Chang HD, Chiarolla CM*, et al.* Deep phenotypical characterization of human CD3(+) CD56(+) T cells by mass cytometry. Eur J Immunol **2021**;51:672-81
146. Chan WK, Rujkijyanont P, Neale G, Yang J, Bari R, Das Gupta N*, et al.* Multiplex and genome-wide analyses reveal distinctive properties of KIR+ and CD56+ T cells in human blood. J Immunol **2013**;191:1625-36
147. Björkbacka H, Berg KE, Manjer J, Engelbertsen D, Wigren M, Ljungcrantz I*, et al.* CD4+ CD56+ natural killer T-like cells secreting interferon-γ are associated with incident coronary events. J Intern Med **2016**;279:78-88
148. Van Acker HH, Capsomidis A, Smits EL, Van Tendeloo VF. CD56 in the Immune System: More Than a Marker for Cytotoxicity? Front Immunol **2017**;8:892
149. Golden-Mason L, Castelblanco N, O'Farrelly C, Rosen HR. Phenotypic and functional changes of cytotoxic CD56pos natural T cells determine outcome of acute hepatitis C virus infection. J Virol **2007**;81:9292-8
150. Kawarabayashi N, Seki S, Hatsuse K, Ohkawa T, Koike Y, Aihara T*, et al.* Decrease of CD56(+)T cells and natural killer cells in cirrhotic livers with hepatitis C may be involved in their susceptibility to hepatocellular carcinoma. Hepatology **2000**;32:962-9
151. Pang YL, Zhang HG, Peng JR, Pang XW, Yu S, Xing Q*, et al.* The immunosuppressive tumor microenvironment in hepatocellular carcinoma. Cancer Immunol Immunother **2009**;58:877-86
152. Gharagozloo M, Rezaei A, Kalantari H, Bahador A, Hassannejad N, Maracy M*, et al.* Decline in peripheral blood NKG2D+CD3+CD56+ NKT cells in metastatic colorectal cancer patients. Bratisl Lek Listy **2018**;119:6-11
153. Peng LS, Mao FY, Zhao YL, Wang TT, Chen N, Zhang JY*, et al.* Altered phenotypic and functional characteristics of CD3+CD56+ NKT-like cells in human gastric cancer. Oncotarget **2016**;7:55222-30
154. Lundgren S, Micke P, Elebro J, Heby M, Hrynchyk I, Nodin B*, et al.* Topographical Distribution and Spatial Interactions of Innate and Semi-Innate Immune Cells in Pancreatic and Other Periampullary Adenocarcinoma. Front Immunol **2020**;11:558169
155. Al Omar SY, Marshall E, Middleton D, Christmas SE. Increased numbers but functional defects of CD56+CD3+ cells in lung cancer. Int Immunol **2012**;24:409-15
156. Galon J, Costes A, Sanchez-Cabo F, Kirilovsky A, Mlecnik B, Lagorce-Pagès C*, et al.* Type, density, and location of immune cells within human colorectal tumors predict clinical outcome. Science **2006**;313:1960-4
157. Tosolini M, Kirilovsky A, Mlecnik B, Fredriksen T, Mauger S, Bindea G*, et al.* Clinical impact of different classes of infiltrating T cytotoxic and helper cells (Th1, th2, treg, th17) in patients with colorectal cancer. Cancer Res **2011**;71:1263-71
158. El Sissy C, Kirilovsky A, Van den Eynde M, Muşină AM, Anitei MG, Romero A*, et al.* A Diagnostic Biopsy-Adapted Immunoscore Predicts Response to Neoadjuvant Treatment and Selects Patients with Rectal Cancer Eligible for a Watch-and-Wait Strategy. Clin Cancer Res **2020**;26:5198-207
159. Toor SM, Sasidharan Nair V, Saleh R, Taha RZ, Murshed K, Al-Dhaheri M*, et al.* Transcriptome of Tumor-Infiltrating T Cells in Colorectal Cancer Patients Uncovered a Unique Gene Signature in CD4(+) T Cells Associated with Poor Disease-Specific Survival. Vaccines (Basel) **2021**;9
160. Thomson A, Bento DFC, Scurr MJ, Smart K, Somerville MS, Keita Å V*, et al.* Prognostic significance of interleukin-17A-producing colorectal tumour antigen-specific T cells. Br J Cancer **2021**;124:1552-5

161. Bindea G, Mlecnik B, Tosolini M, Kirilovsky A, Waldner M, Obenauf AC*, et al.* Spatiotemporal dynamics of intratumoral immune cells reveal the immune landscape in human cancer. Immunity **2013**;39:782-95
162. Pang F, Yang P, Wang T, Li X, Wu X, Yue R*, et al.* Comprehensive Analysis of Alternative Polyadenylation Events Associated with the Tumor Immune Microenvironment in Colon Adenocarcinoma. Curr Genomics **2023**;24:48-61
163. Liu X, Wang X, Yang Q, Luo L, Liu Z, Ren X*, et al.* Th17 Cells Secrete TWEAK to Trigger Epithelial-Mesenchymal Transition and Promote Colorectal Cancer Liver Metastasis. Cancer Res **2024**;84:1352-71
164. Feng WQ, Zhang YC, Xu ZQ, Yu SY, Huo JT, Tuersun A*, et al.* IL-17A-mediated mitochondrial dysfunction induces pyroptosis in colorectal cancer cells and promotes CD8 + T-cell tumour infiltration. J Transl Med **2023**;21:335
165. Angelova M, Charoentong P, Hackl H, Fischer ML, Snajder R, Krogsdam AM*, et al.* Characterization of the immunophenotypes and antigenomes of colorectal cancers reveals distinct tumor escape mechanisms and novel targets for immunotherapy. Genome Biol **2015**;16:64
166. Saito T, Nishikawa H, Wada H, Nagano Y, Sugiyama D, Atarashi K*, et al.* Two FOXP3(+)CD4(+) T cell subpopulations distinctly control the prognosis of colorectal cancers. Nat Med **2016**;22:679-84
167. Bergsland CH, Jeanmougin M, Moosavi SH, Svindland A, Bruun J, Nesbakken A*, et al.* Spatial analysis and CD25-expression identify regulatory T cells as predictors of a poor prognosis in colorectal cancer. Mod Pathol **2022**;35:1236-46
168. Lam JH, Hong M, Koo SL, Chua CWL, Lim KL, Wee F*, et al.* CD30(+)OX40(+) Treg is associated with improved overall survival in colorectal cancer. Cancer Immunol Immunother **2021**;70:2353-65
169. Overacre-Delgoffe AE, Bumgarner HJ, Cillo AR, Burr AHP, Tometich JT, Bhattacharjee A*, et al.* Microbiota-specific T follicular helper cells drive tertiary lymphoid structures and anti-tumor immunity against colorectal cancer. Immunity **2021**;54:2812-24.e4
170. Duhen R, Fesneau O, Samson KA, Frye AK, Beymer M, Rajamanickam V*, et al.* PD-1 and ICOS coexpression identifies tumor-reactive CD4+ T cells in human solid tumors. J Clin Invest **2022**;132
171. Chaput N, Louafi S, Bardier A, Charlotte F, Vaillant JC, Ménégaux F*, et al.* Identification of CD8+CD25+Foxp3+ suppressive T cells in colorectal cancer tissue. Gut **2009**;58:520-9
172. Mutala LB, Deleine C, Karakachoff M, Dansette D, Ducoin K, Oger R*, et al.* The Caspase-1/IL-18 Axis of the Inflammasome in Tumor Cells: A Modulator of the Th1/Tc1 Response of Tumor-Infiltrating T Lymphocytes in Colorectal Cancer. Cancers (Basel) **2021**;13
173. Huber M, Heink S, Grothe H, Guralnik A, Reinhard K, Elflein K*, et al.* A Th17-like developmental process leads to CD8(+) Tc17 cells with reduced cytotoxic activity. Eur J Immunol **2009**;39:1716-25
174. Yamashita M, Kimura M, Kubo M, Shimizu C, Tada T, Perlmutter RM*, et al.* T cell antigen receptor-mediated activation of the Ras/mitogen-activated protein kinase pathway controls interleukin 4 receptor function and type-2 helper T cell differentiation. Proc Natl Acad Sci U S A **1999**;96:1024-9
175. Kononen J, Bubendorf L, Kallioniemi A, Bärlund M, Schraml P, Leighton S*, et al.* Tissue microarrays for high-throughput molecular profiling of tumor specimens. Nat Med **1998**;4:844-7
176. Bady E, Möller K, Mandelkow T, Raedler JB, Yang C, Ebner J*, et al.* BLEACH&STAIN 15-marker Multiplexed Imaging in 3,098 Human Carcinomas Reveals Six Major PD-L1-driven Immune Phenotypes with Distinct Spatial Orchestration. Mol Cancer Res **2023**;21:605-13
177. Dum D, Henke TLC, Mandelkow T, Yang C, Bady E, Raedler JB*, et al.* Semi-automated validation and quantification of CTLA-4 in 90 different tumor entities using multiple antibodies and artificial intelligence. Lab Invest **2022**;102:650-7
178. Uhlen M, Bandrowski A, Carr S, Edwards A, Ellenberg J, Lundberg E*, et al.* A proposal for validation of antibodies. Nat Methods **2016**;13:823-7

179. Foundation PS. 2021 Python Language Reference. Available from: http://www.python.org.
180. Blessin NC, Yang C, Mandelkow T, Raedler JB, Li W, Bady E*, et al.* Automated Ki-67 labeling index assessment in prostate cancer using artificial intelligence and multiplex fluorescence immunohistochemistry. J Pathol **2023**;260:5-16
181. R-Core-Team. 2021 R: A language and environment for statistical computing. Available from: https://www.R-project.org/.
182. Yang C, Mandelkow T, Bady E, Raedler JB, Simon R, Sauter G*, et al.* Nonredundant Upregulation of CD112R (PVRIG) and PD-1 on Cytotoxic T Lymphocytes Located in T Cell Nests of Colorectal Cancer. Mod Pathol **2023**;36:100089
183. Debatin NF, Bady E, Mandelkow T, Huang Z, Lurati MCJ, Raedler JB*, et al.* Prognostic Impact and Spatial Interplay of Immune Cells in Urothelial Cancer. Eur Urol **2024**;86:42-51
184. Angell HK, Bruni D, Barrett JC, Herbst R, Galon J. The Immunoscore: Colon Cancer and Beyond. Clin Cancer Res **2020**;26:332-9
185. Tippmann S. Programming tools: Adventures with R. Nature **2015**;517:109-10
186. JMP® V. 1989-2019 SAS Institute Inc., Cary, NC. Available from: https://www.jmp.com.
187. Samusik N, Good Z, Spitzer MH, Davis KL, Nolan GP. Automated mapping of phenotype space with single-cell data. Nat Methods **2016**;13:493-6
188. Llosa NJ, Cruise M, Tam A, Wicks EC, Hechenbleikner EM, Taube JM*, et al.* The vigorous immune microenvironment of microsatellite instable colon cancer is balanced by multiple counter-inhibitory checkpoints. Cancer Discov **2015**;5:43-51
189. Zhang L, Yu X, Zheng L, Zhang Y, Li Y, Fang Q*, et al.* Lineage tracking reveals dynamic relationships of T cells in colorectal cancer. Nature **2018**;564:268-72
190. Toor SM, Sasidharan Nair V, Murshed K, Abu Nada M, Elkord E. Tumor-Infiltrating Lymphoid Cells in Colorectal Cancer Patients with Varying Disease Stages and Microsatellite Instability-High/Stable Tumors. Vaccines (Basel) **2021**;9
191. Chamoto K, Kosaka A, Tsuji T, Matsuzaki J, Sato T, Takeshima T*, et al.* Critical role of the Th1/Tc1 circuit for the generation of tumor-specific CTL during tumor eradication in vivo by Th1-cell therapy. Cancer Sci **2003**;94:924-8
192. Zitvogel L, Kroemer G. CD103+ dendritic cells producing interleukin-12 in anticancer immunosurveillance. Cancer Cell **2014**;26:591-3
193. Broz ML, Binnewies M, Boldajipour B, Nelson AE, Pollack JL, Erle DJ*, et al.* Dissecting the tumor myeloid compartment reveals rare activating antigen-presenting cells critical for T cell immunity. Cancer Cell **2014**;26:638-52
194. Inamdar S, Suresh AP, Mangal JL, Ng ND, Sundem A, Wu C*, et al.* Rescue of dendritic cells from glycolysis inhibition improves cancer immunotherapy in mice. Nat Commun **2023**;14:5333
195. Formentini A, Braun P, Fricke H, Link KH, Henne-Bruns D, Kornmann M. Expression of interleukin-4 and interleukin-13 and their receptors in colorectal cancer. Int J Colorectal Dis **2012**;27:1369-76
196. Liu H, Antony S, Roy K, Juhasz A, Wu Y, Lu J*, et al.* Interleukin-4 and interleukin-13 increase NADPH oxidase 1-related proliferation of human colon cancer cells. Oncotarget **2017**;8:38113-35
197. Aspord C, Leccia MT, Charles J, Plumas J. Plasmacytoid dendritic cells support melanoma progression by promoting Th2 and regulatory immunity through OX40L and ICOSL. Cancer Immunol Res **2013**;1:402-15
198. Tussiwand R, Everts B, Grajales-Reyes GE, Kretzer NM, Iwata A, Bagaitkar J*, et al.* Klf4 expression in conventional dendritic cells is required for T helper 2 cell responses. Immunity **2015**;42:916-28
199. Debatin NF, Bady E, Mandelkow T, Huang Z, Lurati MCJ, Raedler JB*, et al.* Prognostic Impact and Spatial Interplay of Immune Cells in Urothelial Cancer. Eur Urol **2024**;86:42-51
200. Duraiswamy J, Turrini R, Minasyan A, Barras D, Crespo I, Grimm AJ*, et al.* Myeloid antigen-presenting cell niches sustain antitumor T cells and license PD-1 blockade via CD28 costimulation. Cancer Cell **2021**;39:1623-42 e20

201. Solinas C, Garaud S, De Silva P, Boisson A, Van den Eynden G, de Wind A*, et al.* Immune Checkpoint Molecules on Tumor-Infiltrating Lymphocytes and Their Association with Tertiary Lymphoid Structures in Human Breast Cancer. Front Immunol **2017**;8:1412
202. Burandt E, Blessin NC, Rolschewski AC, Lutz F, Mandelkow T, Yang C*, et al.* T-Cell Density at the Invasive Margin and Immune Phenotypes Predict Outcome in Vulvar Squamous Cell Cancer. Cancers (Basel) **2022**;14
203. Bindea G, Mlecnik B, Tosolini M, Kirilovsky A, Waldner M, Obenauf AC*, et al.* Spatiotemporal dynamics of intratumoral immune cells reveal the immune landscape in human cancer. Immunity **2013**;39:782-95
204. Quail DF, Joyce JA. Microenvironmental regulation of tumor progression and metastasis. Nat Med **2013**;19:1423-37
205. Lin JR, Wang S, Coy S, Chen YA, Yapp C, Tyler M*, et al.* Multiplexed 3D atlas of state transitions and immune interaction in colorectal cancer. Cell **2023**;186:363-81 e19

9. Abbreviations

CRC	*Colorectal cancer*
CIN	*Chromosomal Instability*
bfIHC	*brightfield-immunohistochemistry*
DAPI	*Diamidin-2-phenylindol*
i.e.,	*id est*
e.g.,	*exempli gratia*
FDA	*Food and Drug Administration*
HE	*Hematoxylin and eosin*
IFN	*Interferon*
mfIHC	*multiplex-fluorescence-immunohistochemistry*
MSI/dMMR	*Microsatellite instability and/or mismatch-repair deficiency*
MSS/pMMR	*Microsatellite stability and/or mismatch-repair proficient*
mRNA	*messenger* ribonuclear acid
NK-cells	*Natural killer cells*
PD-1	*Programmed cell death protein 1*
PD-L1	*Programmed cell death 1 ligand*
CIMP	*CpG island methylator phenotype*
CMS	*Consensus Molecular Subtypes*
DNA	*Deoxyribonucleic Acid*
PCR	*Polymerase Chain Reaction*
NGS	*next-generation sequencing*
CE	*Capillary Electrophoresis*
MSI-H	*Microsatellite Instability High*
TMB	*Tumor Mutational Burden*
TCGA	*The Cancer Genome Atlas*
M1	*Type 1 macrophage*
M2	*Type 2 macrophage*
TAM	*tumor-associated macrophage*
EMT	*epithelial-mesenchymal transition*
DC	*dendritic cell*
pDC	*plasmacytoid dendritic cell*
TGF-β	*Transforming Growth Factor Beta*
VEGF	*Vascular Endothelial Growth Factor*
MDSC	*Myeloid-derived suppressor cell*

TNM	*tumor-node-metastasis*
CXCL	*CXC Chemokine Ligand*
CXCR	*CXC Chemokine Receptor*
IL	*Interleukin*
KRAS	*Kirsten Rat Sarcoma Viral Oncogene Homolog*
MC	*mast cells*
MMP	*Matrix Metalloproteinase*
CAF	*Cancer-associated fibroblast*
α-SMA	*Alpha-Smooth Muscle Actin*
P4HA1	*Prolyl 4-Hydroxylase Subunit Alpha 1*
LRG1	*Leucine Rich Alpha-2-Glycoprotein 1*
STAT	*Signal Transducer and Activator of Transcription*
CD	*Cluster of Differentiation*
Tc1	*Type 1 cytotoxic T-cell*
Tc2	*Type 2 cytotoxic T-cell*
Tc17	*Type 17 cytotoxic T-cell*
Tcreg	*Regulatory cytotoxic T-cells*
NKT-like cells	*Natural killer T-like cells*
Th1	*Type 1 helper T-cell*
Th2	*Type 2 helper T-cell*
Th17	*Type 17 helper T-cell*
Tfh	*Follicular helper T-cells*
Treg	*Regulatory helper T-cells*
T-bet	*T-box transcription factor*
IFN-γ	*Interferon-gamma*
TNF-α	*Tumor Necrosis Factor Alpha*
GATA-3	*GATA binding protein 3*
RORγt	*Retinoic acid–related orphan receptor gamma t*
Bcl-6	*B-cell lymphoma 6*
CTLA-4	*Cytotoxic T-Lymphocyte Associated Protein 4*
Ki67	*Ki67 Antigen*
panCK	*Pan-Cytokeratin*
HLA-DR	*Human Leukocyte Antigen - DR*
TLS	*tertiary lymphoid structures*
Foxp3	*Forkhead box P3*
EOMES	*Eomesodermin*

Fas	*Fatty acid synthase receptor*
FasL	*Fas ligand*
IgE	*Immunoglobulin E*
TIM3	*T cell immunoglobulin and mucin domain 3*
MAIT	*Mucosal-associated invariant T-cell*
NKG2D	*Natural Killer Group 2 Member D*
NCR	*Natural Cytotoxicity Receptors*
TMA	*tissue microarray*
ME-TMA	*microenvironment-tissue microarray*
MSH	*MutS Homolog*
MLH	*MutL Homolog*
PMS	*Postmeiotic Segregation*
RAS	*Rat Sarcoma*
HER2	*Human Epidermal Growth Factor Receptor 2*
$H_2O_{dest.}$	*distilled water*
TBS	*Tris-buffered saline*
DAB	*Diaminobenzidine*
HRP	*horseradish peroxidase*
TSA	*tyramide signal amplification*
OPAL	*Oligonucleotide Probes for Amplification and Labeling*

10. List of Figures

11. List of Tables

12. Declaration of Own Contribution

I, Zhihao Huang, declare that this doctoral dissertation titled "Tc1 and Th1 T-lymphocyte rich tumor microenvironment is a hallmark of MSI colorectal cancer" is my own original work. The contributions I made to this research are as follows: 1. Research Design and Conceptualization. Under the guidence of supervisors, I formulated the research questions and hypotheses that guided this study, ensuring alignment with current research issues in T-cell composition in tumor immune microenvironment of MSI colorectal cancer. 2. Literature Review: I conducted a thorough literature review, identifying and synthesizing relevant studies to establish the theoretical foundation of this research. 3. Methodology Development: I developed some new research methodology, including statistical analyses or graphing methods appropriate for this study. 4. Data Analysis: I performed data analyses using R version 3.6.1 and JMP Pro 17, interpreting the results to derive meaningful conclusions. 5. Interpretation of Results: I analyzed and discussed the implications of the findings, contributing unique insights relevant to the underliying changes of T-cell composition of MSI colorectal cancers. 6. Manuscript Writing: I wrote the dissertation, including all chapters and sections, incorporating feedback from my supervisor and committee. I acknowledge the guidance and contributions of my supervisor, Prof. Sauter, and colleagues, but affirm that the original work presented here is my own. This dissertation has not been submitted for any other degree or qualification.

13. Eidesstattliche Versicherung

Ich versichere ausdrücklich, dass ich die Arbeit selbständig und ohne fremde Hilfe, insbesondere ohne entgeltliche Hilfe von Vermittlungs- und Beratungsdiensten, verfasst, andere als die von mir angegebenen Quellen und Hilfsmittel nicht benutzt und die aus den benutzten Werken wörtlich oder inhaltlich entnommenen Stellen einzeln nach Ausgabe (Auflage und Jahr des Erscheinens), Band und Seite des benutzten Werkes kenntlich gemacht habe. Das gilt insbesondere auch für alle Informationen aus Internetquellen.

Soweit beim Verfassen der Dissertation KI-basierte Tools („Chatbots“) verwendet wurden, versichere ich ausdrücklich, den daraus generierten Anteil deutlich kenntlich gemacht zu haben. Die „Stellungnahme des Präsidiums der Deutschen Forschungsgemeinschaft (DFG) zum Einfluss generativer Modelle für die Text- und Bilderstellung auf die Wissenschaften und das Förderhandeln der DFG“ aus September 2023 wurde dabei beachtet.

Ferner versichere ich, dass ich die Dissertation bisher nicht einem Fachvertreter an einer anderen Hochschule zur Überprüfung vorgelegt oder mich anderweitig um Zulassung zur Promotion beworben habe.

Ich erkläre mich damit einverstanden, dass meine Dissertation vom Dekanat der Medizinischen Fakultät mit einer gängigen Software zur Erkennung von Plagiaten überprüft werden kann.

Datum: 11.12.2024 Unterschrift: Huang Zhihao

14. Acknowledgement

Time has flown by, and nearly three years have passed since I first arrived in Germany. Looking back, I'm filled with gratitude for the people who have supported me throughout this journey—my supervisors, colleagues, friends, and family.

First and foremost, I want to express my deepest thanks to my supervisors, Pro. Sauter and Pro. Simon. I'm incredibly grateful for the invitation they extended to me, giving me the chance to study in Germany and pursue my MD degree. Their guidance and support have been invaluable across my three main projects and the writing of my dissertation. As I neared graduation, Pro. Sauter provided valuable advice on finalizing each manuscript. I'd also like to thank him for the opportunity to attend an international conference in the USA, which was a deeply enriching experience.

I'm also very grateful to Dr. Blessin, my direct supervisor, for his support both academically and personally. During my early days in Germany, he helped me adjust to life here and taught me the foundational techniques I'd need for my research. He guided me through collaborative projects and encouraged me as I developed my own independent research. I could always count on him for detailed discussions whenever I needed, which made a big difference in the progress of my work.

I'd also like to thank my colleagues—Tim, Elena, Jan, Julia, and Monika—for their friendship and support. Tim helped a lot with my second project, and Elena was incredibly patient in teaching me the basics when I first started, which helped me settle in quickly. She also continued to support me through all three projects and the dissertation writing. I'm thankful to Jan for his technical advice and our interesting discussions about current events and politics. I appreciate Julia's help with staining and scanning across all my projects and Monika's assistance with the same in my third project.

Finally, I want to thank my girlfriend, Zhengxi. Her support and understanding have been a constant source of encouragement, helping me find confidence during tough times. She's been a real motivator in my life. I'm also deeply grateful to my parents, who, despite the distance, have shown unwavering support and care for my well-being and studies.